Engineering Structures 234 (2021) 111949

Contents lists available at ScienceDirect

Engineering Structures

journal homepage: www.elsevier.com/locate/engstruct

The influence of transverse reinforcement and yielding of flexural reinforcement on the shear-transfer actions of RC members

Andrea Monserrat López [a,*], Miguel Fernánez Ruiz [b], Pedro Fco Miguel Sosa [a]

[a] Universitat Politècnica de València, Camí de Vera s/n, 46022 Valencia, Spain
[b] École Polytechnique Fédérale de Lausanne, ENAC, Station 18, CH-1015 Lausanne, Switzerland

ARTICLE INFO

Keywords:
Shear strength
Reinforced concrete
Shear reinforcement
Cantilever
Continuous beam
Digital image correlation
Shear-transfer actions

ABSTRACT

The assessment of the shear strength of reinforced concrete beams with and without shear reinforcement is investigated in this paper on the basis of the contribution of the various potential shear-transfer actions. To that aim, a comprehensive experimental programme is presented, aimed at representing realistic conditions in reinforced concrete members. The programme comprised 15 cantilevers and 15 continuous beams with and without stirrups. In addition, some of the tests were designed to fail in shear after yielding of the flexural reinforcement, allowing to investigate on the structural implications of this phenomenon. The tests were instrumented by means of surface measurements using Digital Image Correlation (DIC), tracking in a detailed manner the development and kinematics of the critical shear crack leading to failure. Based on these measurements, and by accounting for suitable constitutive models, the contribution of the shear-transfer actions is estimated at different levels of load.

The comparison of the experimental results with the calculated shear strength (sum of the contribution of the various shear-transfer actions at failure) shows consistent agreement for the various cases investigated. On this basis, several conclusions about the dominant shear-transfer actions at shear failure are presented, particularly on the role of the shear reinforcement and on the implications of the flexural reinforcement yielding on the overall response.

1. Introduction

Research on the shear strength of reinforced concrete members has been remarkable over the last decades and it has involved extensive experimental and theoretical work. The design approaches based on these works have traditionally been different for members with and without shear reinforcement. For members with shear reinforcement, equilibrium-based models [1,2] (extended from the truss analogy [3–5]) and stress fields [6] are acknowledged as sound and safe approaches. They provide freedom for the necessary design choices and allow for consistent design of beam regions (dominated by the Bernouilli-Navier response) and discontinuity regions (where nonlinear strain distributions occur). Other approaches are also widely extended for design of members with shear reinforcement, as the Modified Compression Field Theory (MCFT) [7–8], Softened Truss Models [9–10] or others [11,12].

For members without shear reinforcement, a rational explanation for the phenomena governing the shear strength has been a matter of debate, and design expressions have traditionally been based on empirical formulas calibrated on the basis of experimental results [13,14]. In order to make a step forward in this field, a number of efforts have been devoted to the understanding of the role of shear-transfer action on cracked concrete. Such contributions refer to aggregate interlock [15–22] (V_{agg} in Fig. 1), dowel action [23–28] (V_{dow} in Fig. 1) and the residual tensile strength of concrete [29–31] (V_{res} in Fig. 1). Also, the contribution of the inclination of the compression chord to the shear transfer (V_{cc} in Fig. 1) has been acknowledged as a significant action in some cases, particularly for members with low slenderness [28,32,33]. In this work, this contribution is obtained at the vertical section defined by the observed tip of the critical shear crack and the outermost compressive fibre of the section (Fig. 1). However, it must be pointed out that some authors ([32,34–40]) consider this vertical section as the one defined by the point where the crack turns (neutral axis) and the outermost compressive fibre of the section.

Some approaches accounting for the role of the various shear-transfer actions have been proposed so far, as the Critical Shear Crack Theory [41,42] or the works by Marí et al. [38,43]. These approaches, accounting for the various shear-transfer actions, present some

* Corresponding author.
E-mail address: anmonlo6@upv.es (A. Monserrat López).

https://doi.org/10.1016/j.engstruct.2021.111949
Received 16 July 2020; Received in revised form 23 December 2020; Accepted 20 January 2021
Available online 15 February 2021

Nomenclature

a	shear span (defined as $M_{1,R}/V_{R,test}$)
b	concrete section width
c	concrete cover
c_1	constant of the concrete residual tensile strength model
c_2,c_3,c_4	constants of the aggregate interlock model
c_m	thickness of the compressive stress block at the edge of the loading plate ($c_m = c_{m1} + c_{m2}$)
c_{m1}	thickness of the block of compressive stresses generated at the edge of the loading plate
c_{m2}	thickness of the block of compressive stresses generated at the edge of the loading plate by N_{cc}
c_n	distance from the bottom compression fibre to the axis where the inclined force of the compression chord acts
d	effective depth (distance from the extreme compression fibre to the centroid of the tensile flexural reinforcement)
d_{dg}	average roughness
d_g	maximum aggregate size
f_c	compressive strength of concrete measured in cylinder
f_{ct}	tensile strength of concrete
f_u	tensile strength of reinforcement
f_y	yield strength of reinforcement
h	concrete section height
h_T	thickness of the compression zone below the tip of the critical shear crack
l'	shear span in continuous beams (defined as $(M_{1,R} + M_{2,R})/V_{R,test}$)
$l_{cont,i}$	tributary length of the crack i
l_{dow}	horizontal length affected by dowelling action
l_j	distance between crack i and the point j
l_k	distance between crack i and the point k
l_{tot}	total specimen length
l_x	cantilever length (x = 1, 3) or span (x = 2)
l_{xx}	segment of the span (xx = a, b, c)
m	linear gradient of stress prior to yielding of reinforcement
m_y	linear gradient of stress after yielding of reinforcement
r_T	horizontal distance from the edge of the loading plate to the tip of the critical shear crack
w	crack width normal to the crack
$\overline{w}$	normalised crack opening
w_0	initial crack opening
w_{lim}	maximum crack opening allowing tensile stresses transfer in concrete
x_{dow}	distance from the points that define de length affected by dowelling action to the external points used to calculate this action
A_s	area of tensile flexural reinforcement
A_s'	area of compressive flexural reinforcement
A_{sw}	area of shear reinforcement
E_s	modulus of elasticity of steel reinforcement
G_F	fracture energy
M	bending moment
$M_{1,R}$	absolute value of bending moment at failure (at A support section in cantilever tests and at B support section in continuous beam tests)
$M_{2,R}$	bending moment at failure (at section of applied load P_2 in continuous beam tests)
N_{cc}	horizontal force carried by inclined compression chord
P_x	applied load (x = 1,2)
R_A	reaction in support section A
R_B	reaction in support section B
V	shear force
V_{agg}	shear force carried by aggregate interlock
V_{calc}	shear force carried by the various shear-transfer actions
V_{cc}	shear force carried by inclined compression chord
V_{dow}	shear force carried by dowel action
$V_{dow,c}$	shear force carried by dowel action (compressive flexural reinforcement)
$V_{dow,t}$	shear force carried by dowel action (tensile flexural reinforcement)
$V_{p,test}$	shear at the peak load in tests
V_{res}	shear force carried by concrete residual tensile strength
$V_{R,calc}$	shear force carried by the various shear-transfer actions at failure
$V_{R,test}$	shear strength in tests
V_s	shear force carried by shear reinforcement
V_{sw}	shear force carried by a stirrup
α_{cc}	inclination of the compression chord
β	inclination of a segment of the polyline that approximates the shape of the critical shear crack
γ	crack opening angle
δ	crack sliding
$\overline{\delta}$	normalized crack sliding
δ_b	relative concrete-to-steel slip
δ_{by}	relative concrete-to-steel slip at yielding
δ_i	specimen deflection under applied load (i = 1,2)
ε_s	strain of a reinforcing bar
$\varepsilon_{s,c}$	strain at the central axis of a reinforcing bar
ε_{sw}	strain of a stirrup
ε_u	strain at maximum load of reinforcement
ε_y	yield strain of reinforcement
$\nu_{sw,i}$	vertical crack opening of the crack i at the location where it intercepts a stirrup
ξ	integration variable of aggregate interlock and residual tensile stresses
ρ	reinforcement ratio of flexural reinforcement
ρ_w	reinforcement ratio of shear reinforcement
σ_{agg}	aggregate interlock normal stress
σ_c	concrete compressive stress in the compressive stress block at the edge of the loading plate
σ_{res}	concrete residual tensile stress
σ_s	stress of a reinforcing bar
σ_{sw}	stress of a stirrup
τ_{agg}	aggregate interlock shear stress
τ_b	bond stress of reinforcement
τ_{b1}	bond stress prior to yielding of reinforcement
τ_{b2}	bond stress after yielding of reinforcement
υ_{PA}, υ_{PB}	vertical displacement
υ_{PA1}, υ_{PB1}	vertical displacement
υ'_{PA}, υ'_{PB}	slope
ϕ	nominal diameter of a reinforcing bar
χ	section curvature

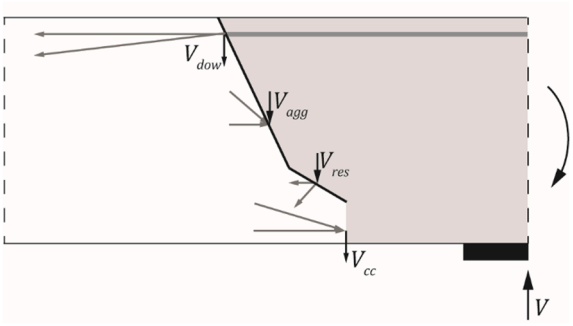

Fig. 1. Shear-transfer actions in a member without shear reinforcement: aggregate interlock (V_{agg}), dowel action (V_{dow}), residual tensile strength (V_{res}) and inclination of the compression chord (V_{cc}).

differences in the role and significance attributed to each action. It is however interesting to note that, despite these differences, the shear strength predictions fit comparably well with experimental results. In order to make a step forward in the understanding of the response of members without stirrups, it is thus instrumental to suitably determine on the basis of test results the role of the different actions and their governing parameters. Significant advances in this field have been performed in the last years [44–46]. Notably, the use of Digital Image Correlation (DIC) [45,46] has allowed providing valuable information about the cracking patterns and associated kinematics during the process of failure. On this basis, accurate analysis of the activation of the various potential shear-transfer actions and their contribution to the member strength can be performed [45,46].

In this paper, following the possibilities offered by DIC, a detailed analysis of the various potential shear-transfer actions is presented for reinforced concrete beams with and without shear reinforcement tested by the authors [47,48]. The tests are part of an extensive experimental programme consisting of 15 cantilever tests and 15 continuous beam tests. The tests aim at representing realistic conditions of reinforced concrete structures both in terms of static system and internal forces (such as those of continuous beams, redundant planar members or cantilevers, refer to Fig. 2). The specimens were instrumented with DIC, used for a detailed tracking of cracking and its associated kinematics. This information, together with suitable constitutive models, allows estimating the amount of force transferred by each shear-transfer action during the process of loading and at failure.

In this work, the presence of shear reinforcement in the response of the member is investigated together with the role of the static system (cantilevers and continuous beams). In particular, some of the tests were designed to fail in shear after yielding of the flexural reinforcement, allowing to investigate in a detailed manner the implications of large

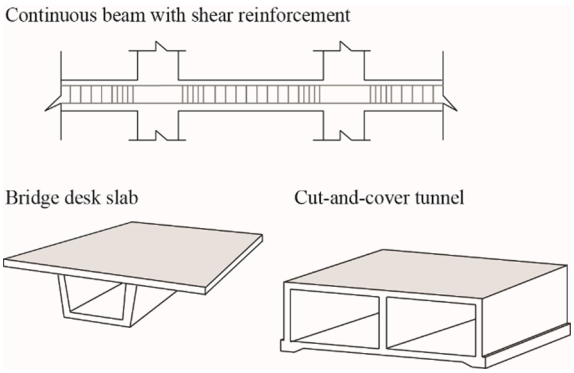

Fig. 2. Examples of reinforced concrete statically indeterminate structures with and without shear reinforcement: continuous beams, cantilever slabs and redundant planar members.

flexural strains on the shear strength (completing previous researches on continuous members [46,49–53]). On the basis of the test results and their analysis, a number of implications for future development of design models are highlighted and discussed.

2. Experimental programme

2.1. Specimens and test procedure

The experimental programme was presented in detail in Monserrat López et al. [47,48]. It comprised 30 different shear tests conducted on 15 reinforced concrete beams (specimens B1 to B15, see Table 1). Each of these 15 beams was tested under two different load configurations (giving rise to 15 cantilever tests and 15 tests on continuous beams, see Fig. 3a and Fig. 3b).

Specimens B1 to B9 were 9.00 m long and B10 to B15 were 7.00 m long. All of them had a rectangular cross section of 250 × 450 mm (see Fig. 3c). Three series were considered according to the shear reinforcement ratio: beams without shear reinforcement (series R0); beams with a shear reinforcement ratio ρ_w = 0.13% (series R1, two-legged closed stirrups ϕ8/30) and beams with a shear reinforcement ratio ρ_w = 0.20% (series R2, two-legged closed stirrups ϕ8/20). Outside of the expected failure regions, stirrups were provided to prevent shear failures (ρ_w = 0.90% in all specimens). Three ratios were considered with respect to the flexural reinforcement: ρ = 1.63% (section S1, effective depth d = 386 mm); ρ = 2.29% (section S2, effective depth d = 385 mm); ρ = 1.94% (section S3, effective depth d = 389 mm). All sections had a total of twelve 20 mm-diameter bars arranged as tensile (top) and compressive (bottom) flexural reinforcement (arranged in two layers, see Fig. 3c). The specimens were tested under different configurations of load and support points. In the cantilever tests, the length of cantilever l_1 was 1.00 m (L1), 1.62 m (L1.6) and 2.31 m (L2.3) (see Fig. 3a); in the continuous beam tests, the length of the span l_2 was 6.00 m (L6), 5.00 m (L5) and 4.00 m (L4) (see Fig. 3b).

The name of the specimens and tests was provided to allow an easy identification of its parameters. It is composed of four terms in the following order: (1) specimen (B1 to B15) and type of test (C -cantilever- for the cantilever test and S -span- for the continuous beam test); (2) series according to the shear reinforcement ratio (R0, R1 or R2); (3) section according to the flexural reinforcement ratio (S1, S2 or S3); (4) length of the cantilever (L1, L1.6 or L2.3) or length of the span (L6, L5 or L4) according to the cantilever or continuous beam test, respectively. Table 1 summarizes the reinforcement, geometry and material properties of all tests.

With respect to the test procedure, in cantilever tests (Fig. 3a), load P_1 was applied with displacement control until shear failure occurred. In these tests, load P_2 was applied with load control according to P_1 to obtain no reaction at support*B*. The continuous beam tests (Fig. 3b) were carried out in two phases, taking advantage of the cantilever that was not tested previously (see Fig. 3a). In the first phase, load P_1 was applied with displacement control, and load P_2 with load control according to P_1 to obtain no reaction at support *A*. This phase ended when the top flexural reinforcement at the support *B* section yielded. In the second phase, load P_2 was applied with displacement control until shear failure, and load P_1 was controlled to keep the slope at the support *B* constant and equal to the one at the end of the first phase. To maintain such slope, it was observed that a limited increase of load P_1 was required, which was responsible for additional rotations in the plastic hinge (due to the increasing rotation of the inner span).

All specimens were cast with normal-strength concrete with maximum aggregate size d_g of 10 mm (the low-size aggregate was used to facilitate concrete casting due to the narrow spacing between bars). The concrete cylinder compressive strength (f_c measured on cylinders with a diameter of 150 mm and a height of 300 mm) and tensile strength (f_{ct} measured on indirect tensile tests on cylinders with a diameter of 150 mm and a height of 300 mm) at the time of testing are included in

Table 1
Reinforcement, geometry and material properties of all tests.

Specimen	Tests	A_s	$A_s^{'}$	ρ(%)	A_{sw}	l_{tot}(m)	l_1(m)	l_2(m)	l_3(m)	l_a(m)	l_b(m)	l_c(m)	f_c(MPa)	f_{ct}(MPa)
B1	B1C-R1-S1-L1 B1S-R1-S1-L6	5ϕ20	7ϕ20	1.63	ϕ8/30	9.00	1.00	6.00	1.00	1.00	3.10	1.90	24.1	2.5
B2	B2C-R1-S2-L1 B2S-R1-S2-L6	7ϕ20	5ϕ20	2.29	ϕ8/30	9.00	1.00	6.00	1.00	1.00	2.50	2.50	22.3	3.1
B3	B3C-R1-S3-L1 B3S-R1-S3-L6	6ϕ20	6ϕ20	1.94	ϕ8/30	9.00	1.00	6.00	1.00	1.00	2.80	2.20	22.8	2.8
B4	B4C-R1-S1-L1.6 B4S-R1-S1-L5	5ϕ20	7ϕ20	1.63	ϕ8/30	9.00	1.62	5.00	1.00	1.00	2.10	1.90	22.3	2.6
B5	B5C-R1-S2-L1.6 B5S-R1-S2-L5	7ϕ20	5ϕ20	2.29	ϕ8/30	9.00	1.62	5.00	1.00	1.00	1.50	2.50	34.7	3.6
B6	B6C-R1-S3-L1.6 B6S-R1-S3-L5	6ϕ20	6ϕ20	1.94	ϕ8/30	9.00	1.62	5.00	1.00	1.00	1.80	2.20	35.9	3.3
B7	B7C-R1-S1-L2.3 B7S-R1-S1-L4	5ϕ20	7ϕ20	1.63	ϕ8/30	9.00	2.31	4.00	1.00	1.00	1.10	1.90	36.2	2.9
B8	B8C-R1-S2-L2.3 B8S-R1-S2-L4	7ϕ20	5ϕ20	2.29	ϕ8/30	9.00	2.31	4.00	1.00	1.00	0.50	2.50	34.5	3.4
B9	B9C-R1-S3-L2.3 B9S-R1-S3-L4	6ϕ20	6ϕ20	1.94	ϕ8/30	9.00	2.31	4.00	1.00	1.00	0.80	2.20	29.7	2.2
B10	B10C-R0-S1-L1 B10S-R0-S1-L4	5ϕ20	7ϕ20	1.63	–	7.00	1.00	4.00	1.00	0.70	1.40	1.90	36.4	2.1
B11	B11C-R0-S2-L1 B11S-R0-S2-L4	7ϕ20	5ϕ20	2.29	–	7.00	1.00	4.00	1.00	1.00	0.61	2.50	31.4	2.1
B12	B12C-R0-S3-L1 B12S-R0-S3-L4	6ϕ20	6ϕ20	1.94	–	7.00	1.00	4.00	1.00	0.89	0.91	2.20	28.7	2.9
B13	B13C-R2-S1-L1 B13S-R2-S1-L4	5ϕ20	7ϕ20	1.63	ϕ8/20	7.00	1.00	4.00	1.00	1.00	1.10	1.90	30.6	2.5
B14	B14C-R2-S2-L1 B14S-R2-S2-L4	7ϕ20	5ϕ20	2.29	ϕ8/20	7.00	1.00	4.00	1.00	1.00	0.50	2.50	31.4	2.9
B15	B15C-R2-S3-L1 B15S-R2-S3-L4	6ϕ20	6ϕ20	1.94	ϕ8/20	7.00	1.00	4.00	1.00	1.00	0.80	2.20	26.0	2.6

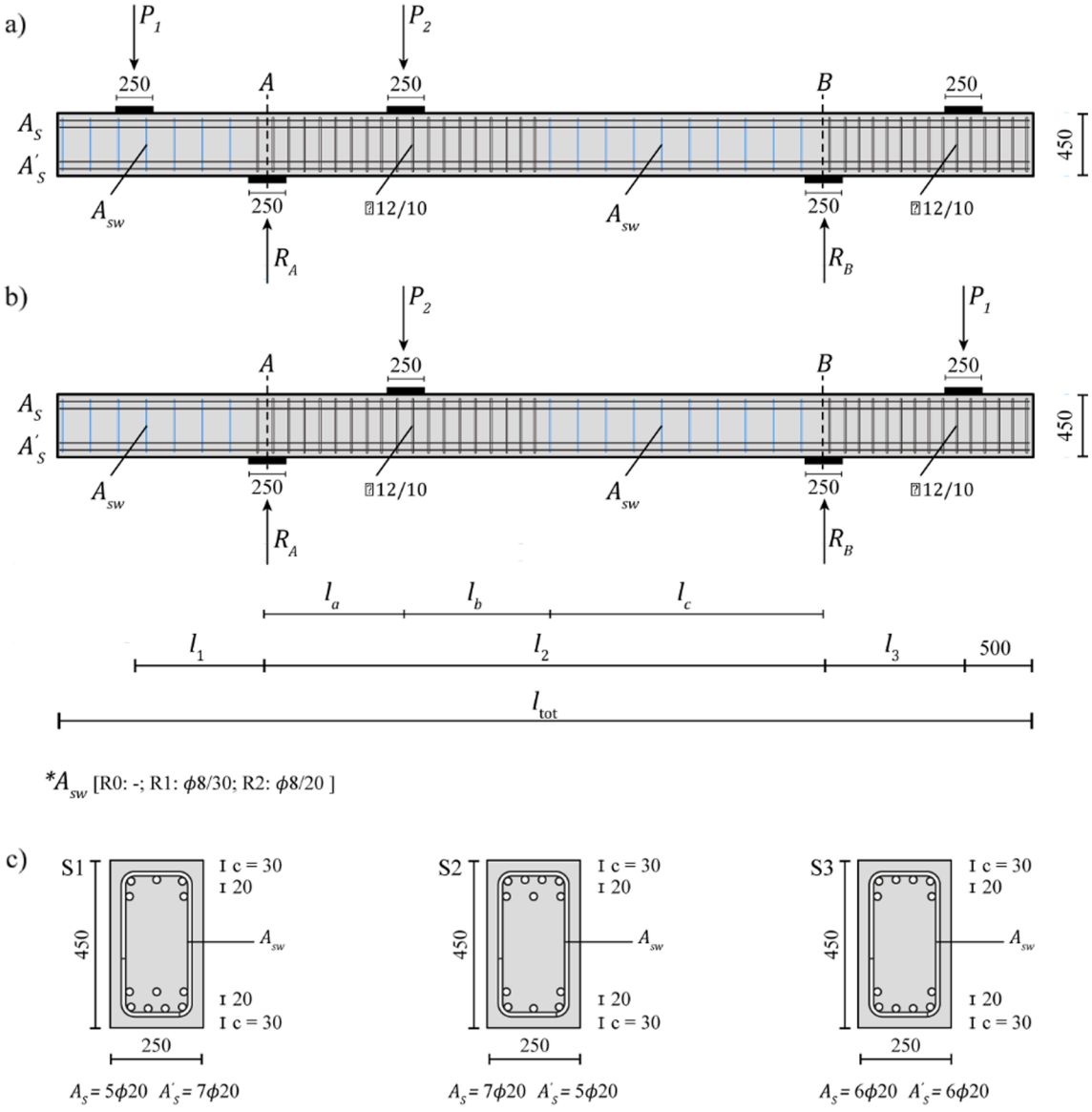

Fig. 3. Reinforcement, geometry and load arrangement of the specimens in (a) cantilever test and (b) continuous beam test; (c) flexural reinforcement of sections S1, S2 and S3 (dimensions in mm).

Table 1. The reinforcement steel properties are summarized in Table 2.

2.2. Photogrammetric measurements (DIC)

Several load, displacement and strain measurements were recorded with conventional instrumentation, such as load cells, displacement transducers and strain gauges [47]. In addition to these conventional measurements, two-dimensional DIC was used to track the cracking pattern and the displacement field of the specimens. Photogrammetry was performed on the specimens' surface, only on the regions where shear failure was expected. To this aim, three or four (depending on the test) Canon EOS 5D Mark II digital cameras (21.1 megapixels) equipped with a fixed-focus lens Canon EF 85 mm f/1.8 USM were used. In the measurement regions, a pattern consisting of rounded black speckles was applied. The image acquisition rate during tests was variable. At the beginning, images were taken every two seconds, but the frequency was increased up to 1 Hz near failure. The DIC software used to obtain the kinematics of the critical shear crack was VIC2D [54]. The calibration was made by the software from an initial reference image with 1-mm dots aligned to a distance of 10 mm. For measuring displacements, images were divided into a grid of facets and each one was tracked from one image to the following to measure the displacement field. From the displacement data provided, it was possible to obtain the kinematics of the critical shear crack, which was essential to obtain the contribution of the various shear-transfer actions. The DIC software used to obtain the critical shear crack opening along the vertical direction at the location where the crack intercepted the different stirrups was different to VIC2D. The isolated measurements were obtained from an own software developed using NI-IMAQ driver and programming with LabVIEW [47]. Images were divided into a grid of squared facets of 100 × 100 pixels to track displacements between them. The software maximum error of the computed displacements was 1/32 pixels. The calibration was done with the Vision Assistant of National Instruments software, and took into account the distortion and projection parameters so that each calibration was valid only for one camera in a specific test. Image calibration was carried out with a dot grid and the obtained resolution was 0.2 mm/pixel.

2.3. Main results

Several shear failure modes were observed (Table 3), two for the cantilever tests and two for the continuous beam tests.

- In cantilever tests, specimens L1 and L1.6 failed in shear before yielding of the top flexural reinforcement at the support section *A* (see Fig. 3a). On the other hand, specimens of the tests B8C-R1-S2-L2.3 and B9C-R1-S3-L2.3 failed in shear after yielding of the flexural reinforcement (i.e. shear failure occurred under constant shear force but for increasing deformations). Finally, test B7C-R1-S1-L2.3 failed in bending. The load–deflection curves (load P_1 against the deflection under this load, δ_1) for the specimens of series R1 (with shear reinforcement) and section S3 ($\rho = 1.94\%$) are plotted in Fig. 4a.

Table 2
Average values of the reinforcement steel properties.

Specimens	ϕ(mm)	E_s(GPa)	f_y(MPa)	f_u(MPa)	ε_u(%)	f_u/f_y
B1-B3	8	198	543	677	9.6	1.25
	20	218	557	665	10.9	1.19
B4-B9	8	183	549	651	11.1	1.19
	20	213	540	649	13.5	1.20
B10, B11, B13	8	193	540	642	10.6	1.19
	20	226	544	651	21.5	1.20
B12, B14, B15	8	189	541	662	10.9	1.22
	20	206	531	639	18.3	1.20

- In continuous beam tests, all specimens failed in shear in the second phase of loading (after yielding of the top flexural reinforcement at support section *B*, see Fig. 3b). Two different failure modes were observed depending on the development or not of a second plastic hinge under load P_2 (see Fig. 3b). Specimens L4, and specimen of the test B4S-R1-S1-L5 failed in shear after formation of the first plastic hinge with increasing shear forces. Specimens L6, and specimens of the tests B5S-R1-S2-L5 and B6S-R1-S3-L5 failed in shear after formation of the second plastic hinge (failure for constant shear forces but for increasing plastic deformations). The load–deflection curves (load P_2 against the deflection under this load, δ_2) for specimens of series R1 and section S3 are plotted in Fig. 4b. These curves show a first branch with negative slope and a limited applied load, which corresponds to the first phase of the continuous beam tests.

The shear strength ($V_{R,test}$) provided by tests at failure at the corresponding support section (support section *A* for the cantilever tests and support section *B* for the continuous beam tests, see Fig. 3) is summarized in Table 3. It is also included the normalised shear strength ($V_{R,test}/bd\sqrt{f_c}$) according to the compressive strength of concrete for each test.

The shear slenderness of the specimens influenced both their failure mode and shear strength. For cantilevers, the shear slenderness ratio a/d (shear span $a = M_{1,R}/V_{R,test}$) is presented in Table 3. For the different specimens of series R1 ($\rho_w = 0.13\%$), the shear strength was strongly influenced by the shear slenderness ratio, decreasing for increasing values of a/d (Fig. 5a). Specimens with $a/d \approx 2.5$ and $a/d \approx 4.0$ failed in shear before reaching their flexural strength and developed larger shear strength than specimens with $a/d \approx 5.5$, which attained their flexural strength prior to shear failure. Regarding the influence of the amount of shear reinforcement, specimens of series R0, R1 and R2 with equivalent values of a/d (L1) showed as expected larger shear strength for increasing amounts of shear reinforcement (Fig. 5b). For continuous beams, the shear slenderness ratio l'/d (shear span $l' = (M_{1,R} + M_{2,R})/V_{R,test}$) is presented in Table 3 (values at failure). As already explained in Monserrat et al. [48], the shear span l' is defined as the distance between two loading sections (for the tested continuous beams, l' is the distance between the section of applied load P_2 and the support section *A*, see Fig. 3c). As for parameter a/d in the cantilevers, a trend appeared between the shear strength and the slenderness l'/d in the continuous beam tests (Fig. 5c). For the different specimens of series R1 ($\rho_w = 0.13\%$), the shear strength decreased for increasing values of l'/d. In addition, all specimens with $l'/d \approx 12.0$ and two with $l'/d \approx 10.0$ failed in shear after reaching their flexural strength (i.e. after the development of two plastic hinges). However, all specimens with the lowest shear slenderness ratio ($l'/d \approx 7.5$) failed in shear before developing the second plastic hinge, regardless the amount of shear reinforcement. These specimens, with equivalent values of l'/d (L4), showed the influence of the shear reinforcement ratio as their shear strength increased for increasing amounts of it (Fig. 5d).

2.4. Cracking pattern

Related to the cracking patterns at failure, they developed differently for cantilever and continuous beam tests. In all cantilever tests, cracking started first in the form of vertical flexural cracks near the support section. In most of the tests, as load increased, one of the flexural cracks developed a sub-horizontal branch towards the support section, becoming eventually the critical shear crack (see Fig. 6a). Nevertheless, in some L1 tests (B3C-R1-S3-L1, B11C-R0-S2-L1, B12C-R0-S3-L1 and B15C-R2-S3-L1), the critical shear crack developed as a diagonal crack in the web and its width increased until shear failure (see Fig. 6b). In continuous beam tests, during the first loading phase, mainly flexural cracking was observed, while the critical shear crack (developed from a flexural crack, see Fig. 6a) progressed until shear failure in the second

Table 3
Main test results at failure (failure mode, shear strength and shear slenderness ratio).

Cantilever test	Failure mode	$V_{R,test}$(kN)	$V_{R,test}/bd\sqrt{f_c}$ ($\sqrt{\text{MPa}}$)	a/d	Continuous beam test	Failure mode	$V_{R,test}$(kN)	$V_{R,test}/bd\sqrt{f_c}$($\sqrt{\text{MPa}}$)	l'/d
B1C-R1-S1-L1	V (B)	196.8	0.416	2.58	B1S-R1-S1-L6	V (2 PH)	139.4	0.294	12.30
B2C-R1-S2-L1	V (B)	214.6	0.472	2.58	B2S-R1-S2-L6	V (2 PH)	142.4	0.313	12.35
B3C-R1-S3-L1	V (B)	206.3	0.444	2.56	B3S-R1-S3-L6	V (2 PH)	145.1	0.312	12.23
B4C-R1-S1-L1.6	V (B)	174.2	0.382	4.16	B4S-R1-S1-L5	V (1 PH)	143.1	0.314	9.96
B5C-R1-S2-L1.6	V (B)	215.2	0.379	4.18	B5S-R1-S2-L5	V (2 PH)	188.7	0.333	10.08
B6C-R1-S3-L1.6	V (B)	207.6	0.356	4.13	B6S-R1-S3-L5	V (2 PH)	190.8	0.327	9.98
B7C-R1-S1-L2.3	M	–	–	–	B7S-R1-S1-L4	V (1 PH)	216.3	0.373	7.62
B8C-R1-S2-L2.3	V (A)	167.6	0.297	5.91	B8S-R1-S2-L4	V (1 PH)	200.9	0.356	7.63
B9C-R1-S3-L2.3	V (A)	148.7	0.281	5.84	B9S-R1-S3-L4	V (1 PH)	192.3	0.363	7.54
B10C-R0-S1-L1	V (B)	150.2	0.258	2.57	B10S-R0-S1-L4	V (1 PH)	82.4	0.141	8.07
B11C-R0-S2-L1	V (B)	188.9	0.350	2.58	B11S-R0-S2-L4*	V (1 PH)	92.0	0.171	7.44
B12C-R0-S3-L1	V (B)	120.8	0.232	2.55	B12S-R0-S3-L4	V (1 PH)	87.6	0.168	7.60
B13C-R2-S1-L1	V (B)	235.0	0.440	2.58	B13S-R2-S1-L4	V (1 PH)	217.6	0.407	7.62
B14C-R2-S2-L1	V (B)	267.7	0.496	2.59	B14S-R2-S2-L4	V (1 PH)	222.5	0.412	7.64
B15C-R2-S3-L1	V (B)	281.0	0.566	2.56	B15S-R2-S3-L4	V (1 PH)	199.1	0.401	7.55

Note: V (shear failure); M (bending failure); A (after yielding); B (before yielding); PH (plastic hinge); shear at corresponding support section including self-weight; *test with different configuration [48].

phase.

The observed cracking patterns for the cantilever tests and continuous beam tests of all specimens are shown in Fig. 7. The cracking patterns were significantly influenced by the presence or absence of stirrups. For specimens with shear reinforcement (R1 and R2), the cracks were more evenly distributed than those of specimens without stirrups (R0), where strains largely localized in a single critical shear crack. Horizontal delamination cracks observed in shear-reinforced tests developed after the peak load was reached.

Specimens with shear reinforcement showed in addition larger crack widths than specimens without it, and were associated to a significant vertical displacement. Generally, the critical shear crack developed near to the support section. However, in the test B14S-R2-S2-L4, the critical shear crack was located relatively far from the support.

3. Analysis of shear-transfer actions

In this section, the shear resistance of the specimens is investigated on the basis of the test measurements. To that aim, the contribution of the various potential shear-transfer actions will be analysed considering a free-body defined by the critical shear crack leading eventually to failure. In addition to the shear-transfer actions related to members without stirrups (aggregate interlock, residual tensile strength of concrete, dowel action of the flexural reinforcement and contribution of the compression chord, see Fig. 1), the contribution of the transverse reinforcement (V_s) will also be considered (see Fig. 8a).

In the following, the procedure to estimate the contribution of the various shear-transfer actions to the shear strength of the tested specimens is presented. This contribution is calculated from the critical shear crack kinematics and by using suitable constitutive models and calculation methodologies (according to [44–46]).

3.1. Aggregate interlock

Aggregate interlock allows for a transfer of forces through cracked surfaces by mechanical engagement of the material at the two sides of the crack. As a result of the roughness of the surface (related to the aggregate size) and of the relative displacements of the crack, normal stresses and shear stresses develop and shear forces are transferred. Several approaches have been developed in the past to determine the contact stresses due to aggregate interlocking [17–19,22]. In the following, the considerations of the Two-Phase model originally developed by Walraven [19] will be used. Consistently with previous works [55], the simplified kinematics of Walraven (opening followed by sliding [19]) is replaced by a more general one, considering an initial opening and then a proportional opening and sliding [20,21]. To ease the numerical integration of the results, the simplified formulas developed by Cavagnis et al. [55] calibrated on this basis will be used. The kinematics (refer to Fig. 8b) is defined by an initial crack opening w_0 followed by a combined opening and sliding at an angle γ (as noted by Guidotti [21]). The resulting aggregate interlock interface stresses (normal stresses σ_{agg} and shear stresses τ_{agg}), are thus defined on the basis of the crack opening w and the crack sliding δ as [49]:

$$\sigma_{agg} = \sqrt{f_c}\cdot\frac{c_4\cdot\overline{\delta}^{7/3}}{(c_2\cdot\overline{w})^{3+c_2\cdot\overline{\delta}}} \tag{1}$$

$$\tau_{agg} = \sqrt{f_c}\cdot\frac{c_3\cdot\overline{\delta}^{4/3}}{(c_2\cdot\overline{w})^{1.8+c_2\cdot\overline{\delta}}} \tag{2}$$

where f_c is the compressive strength of concrete; $c_2 = 40$, $c_3 = 35$ and $c_4 = 400$ are constants; $\overline{\delta} = \delta/d_{dg}$ and $\overline{w} = w/d_{dg}$ are the normalized crack sliding and crack opening respectively and d_{dg} is a parameter characterizing the roughness of the crack ($d_{dg} = \min(40\text{ mm}, 16 + d_g)$ for $f_c \leq 60$ MPa, according to [55]).

It shall be noted that the normal stresses (Eq. (1)) only account for the stresses transferred by aggregate interlock, neglecting the contribution of the residual tensile strength. This latter component can be eventually added to the interlock stresses according to the formulation of Cavagnis et al. [55] and will thus be considered separately in this work.

The vertical component of the shear force transferred by the aggregate interlock (V_{agg}) across the critical shear crack of the tested specimens is eventually obtained by integration of the normal stresses (σ_{agg}) and shear stresses (τ_{agg}) according to:

$$V_{agg} = b\cdot\int_{\xi}\left(\tau_{agg}sin\beta - \sigma_{agg}cos\beta\right)d\xi \tag{3}$$

where b is the width of the section, ξ is the integration variable and β is the inclination of every segment of the polyline that approximates the shape of the critical shear crack (see Fig. 8b).

3.2. Concrete residual tensile strength

The concrete residual tensile strength refers to the capacity of cracked concrete to transfer stresses for low crack openings, when the fracture surface is not yet fully developed and some material bridges between the lips of the cracks [29]. Such regions, usually named as Fracture Process Zones (FPZ) are usually located close to the tips of the cracks, where the lowest crack openings are found. Several approaches defining the relationship between the concrete residual tensile stress and

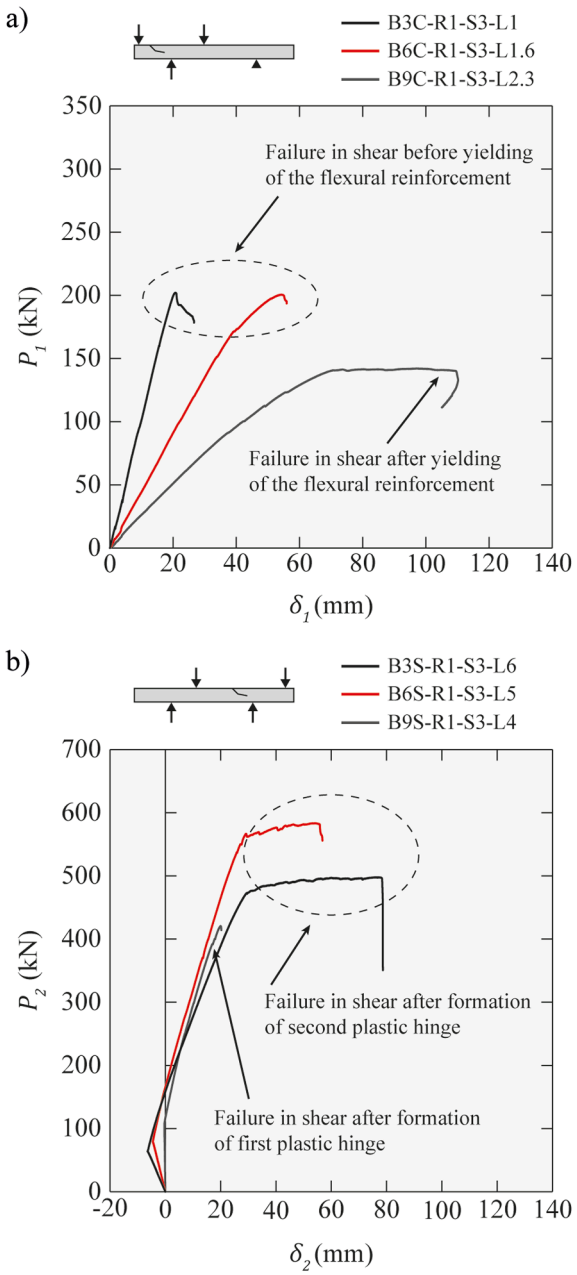

Fig. 4. Load-deflection curves for specimens of series R1 and section S3: (a) cantilever tests; (b) continuous beam tests.

the crack width have been proposed in the past [29–31]. In this work, the expression suggested by Reinhardt [30] (as adopted by Cavagnis et al. [55]) will be used to characterize the residual tensile stresses of concrete:

$$\sigma_{res} = f_{ct} \cdot \left(1 - \left(\frac{w}{w_{lim}}\right)^{c_1}\right) \tag{4}$$

where f_{ct} is the tensile strength of concrete, $c_1 = 0.31$ is a constant, w is the crack width and $w_{lim} = G_F/f_{ct} \cdot (1 + c_1)/c_1$ is the limit crack width for stress transfer. The fracture energy is calculated according to the Model Code 2010 [56] as

$G_F = 0.073 \cdot f_c^{0.18}$, where f_c is the compressive strength of concrete.

For the tested specimens, the values of the limit crack width w_{lim} range from 0.134 mm (specimen B5) to 0.215 mm (specimen B1). By accounting for the actual opening of the cracks, this implies that the contribution of the FPZ remains in general limited to regions close to the crack tips. The residual tensile stress of the crack is thus evaluated for each segment of the crack and the total shear contribution (V_{res}) is calculated by integration of the stresses according to:

$$V_{res} = b \cdot \int_{\xi} \sigma_{res} cos\beta d\xi \tag{5}$$

where b is the width of the section, ξ is the integration variable and β is the inclination of every segment of the polyline that approximates the shape of the critical shear crack (see Fig. 8b).

3.3. Dowel action

The dowel action, or the capacity of the flexural reinforcement to transfer shear forces across a crack, has been investigated in detail by several authors [23–28]. This action is activated by the relative vertical displacements of the crack surfaces at the level of the flexural reinforcement, which requires the development of tensile forces through the concrete cover to ensure the equilibrium of the shear force in the reinforcement [57]. In members without shear reinforcement, these forces develop in the concrete cover and, as a result, the shear resistance due to dowelling action is relatively limited [23–25,28,58]. However, in members with shear reinforcement, the stirrups can efficiently resist to the dowelling forces and increase thus the contribution of this action [44–45].

In this work, the contribution of the dowelling action ($V_{dow,t}$ and $V_{dow,c}$) is obtained on the basis of the measured displacements of the concrete surfaces at the level of the flexural reinforcement consistently with the methodology described in [46]. The deflection of the flexural reinforcement in the horizontal distance influenced by the dowel action (l_{dow}) is approximated by a third-order polynomial (Fig. 9**a**). To that aim, the displacements of four points are obtained for each layer of flexural reinforcement (considering the outer points located at a distance $x_{dow} = \phi/2$, where ϕ refers to the diameter of the bar). Considering the vertical displacements and slopes at the extremities of l_{dow} (v_{PA}, v'_{PA} and v_{PB}, v'_{PB}), the deflection $v(x) = ax^3 + bx^2 + cx + d$ is determined.

Accounting for the shear failures after yielding of the reinforcement (continuous beam tests and cantilever tests B8C-R1-S2-L2.3 and B9C-R1-S3-L2.3), the steel is assumed to have an elastic–plastic response with strain hardening (values in Table 2). The sectional curvature ($\chi(x)$) is obtained by differentiating two times the deflection with respect to x coordinate (Eq. (6)) and the strain of the central axis ($\varepsilon_{s,c}$) of the bar section is calculated from the x coordinate of points PA and PB and the length l_{dow} (Eq. (7)).

$$\chi(x) = \frac{d^2 v(x)}{dx^2} = 6ax + 2b \tag{6}$$

$$\varepsilon_{s,c} = \frac{(x_{PB^{def}} - x_{PA^{def}}) - (x_{PB} - x_{PA})}{l_{dow}} \tag{7}$$

Accounting for the curvature and strain of the bar axis at each section, the bending moment is calculated by considering a planar strain distribution (see Fig. 9b) and the shear force ($V_{dow,t}$, $V_{dow,c}$) is calculated as the derivative of the bending moment.

3.4. Contribution of stirrups

The development of inclined shear cracking in a reinforced concrete member with shear reinforcement leads to the activation of the stirrups intercepted by these cracks and, as a result, shear forces can be carried by them. The contribution of the shear reinforcement (V_s) to the shear strength is obtained from the sum of the shear forces (V_{sw}) carried by each stirrup intercepted by the critical shear crack. In this work, the contribution V_s is obtained following the procedure proposed by Campana et al. [44]. This procedure [44] is based on the measured crack widths and crack locations. At the location where the critical shear crack

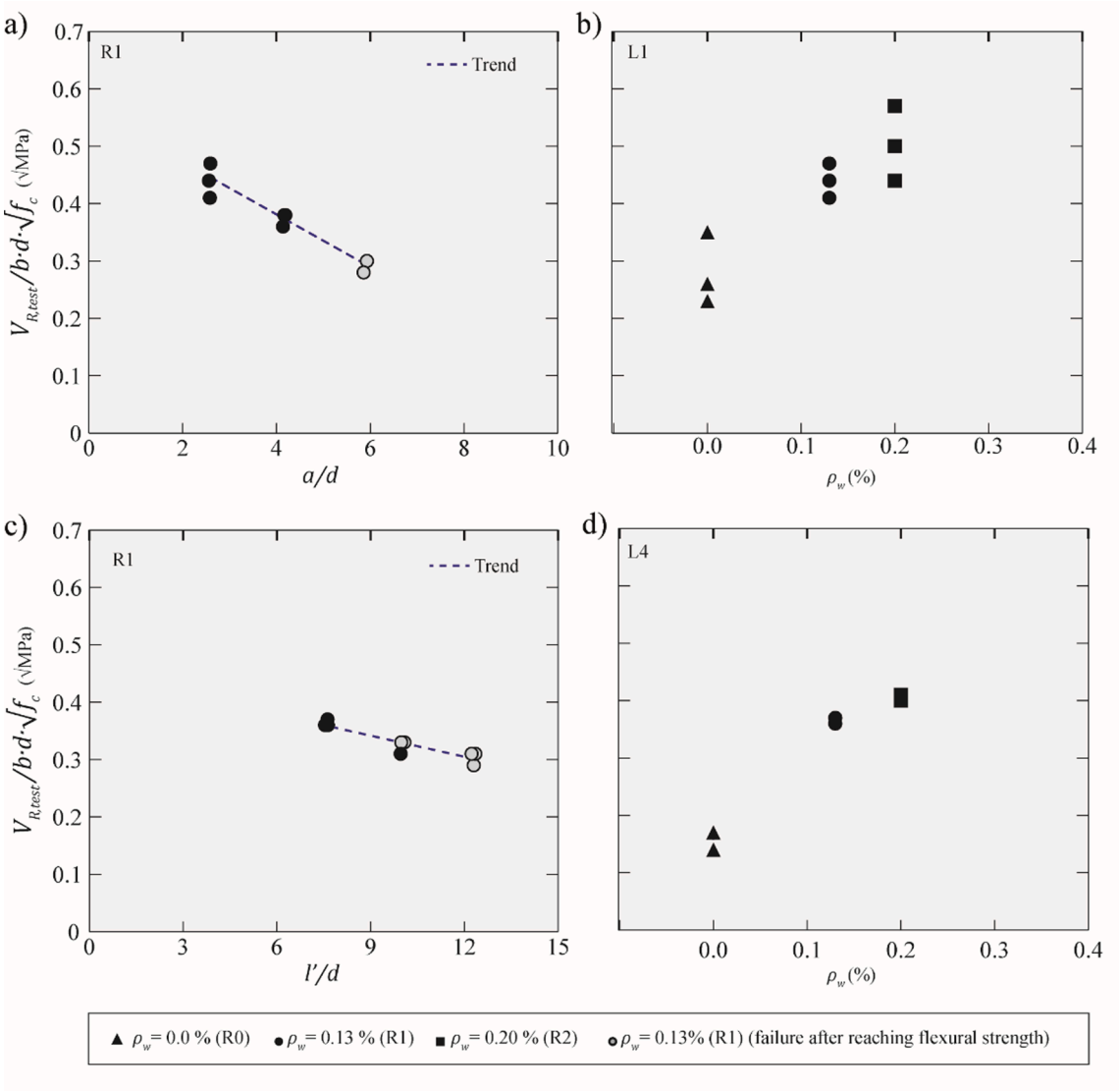

Fig. 5. Shear strength according to the shear slenderness ratio and the shear reinforcement ratio: (a) cantilever tests (R1); (b) cantilever tests (L1); (c) continuous beam tests (R1); continuous beam tests (L4).

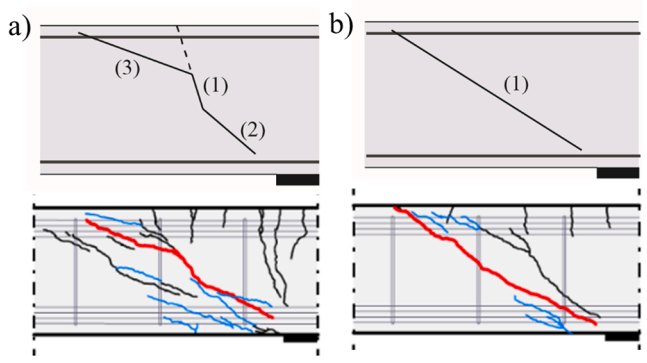

Fig. 6. Crack development process: (a) critical shear crack from a flexural crack (B2C-R1-S2-L1); (b) critical shear crack as a diagonal crack in the web (B3C-R1-S3-L).

(*i*) intercepts each stirrup, its vertical crack opening ($\nu_{sw,i}$) is obtained from the measured displacements of the concrete surfaces at two points (*j* and *k*) vertically aligned with the stirrup (Fig. 10a). Before bar yielding, the constant bond stress is assumed [59] $\tau_{b1} = 2f_{ct}$ and, after yielding, it is reduced to $\tau_{b2} = f_{ct}$ to consider the decreasing bond stress due to the bar lateral contraction [60] (Fig. 10b). On this basis, and by considering a bilinear stress–strain relationship with strain hardening for the steel (Fig. 10c, values in Table 2), the measured crack widths, the stresses (σ_{sw}) and strains (ε_{sw}) in a stirrup are determined, see Fig. 10d. The procedure neglects the concrete strains, so the crack opening ($\nu_{sw,i}$) is obtained by integrating the strains distribution (ε_{sw}) of a stirrup along the tributary length ($l_{cont,i}$) of the crack:

$$\nu_{sw,i} = \int_{l_{cont,i}} \varepsilon_{sw}(x) \cdot dx \tag{8}$$

In this work, the shear force (V_{sw}) carried by each stirrup activated by the critical shear crack is thus calculated from the tensile stress (σ_{sw}) according to:

$$V_{sw} = 2 \cdot \sigma_{sw} \cdot \frac{\phi^2 \cdot \pi}{4} \tag{9}$$

where ϕ is the diameter of the bar (stirrup with two branches) and σ_{sw} is the tensile stress of the stirrup, which is calculated following the procedure of Campana et al. [44]. It can be noted that this procedure neglects the potential kinking of the stirrups.

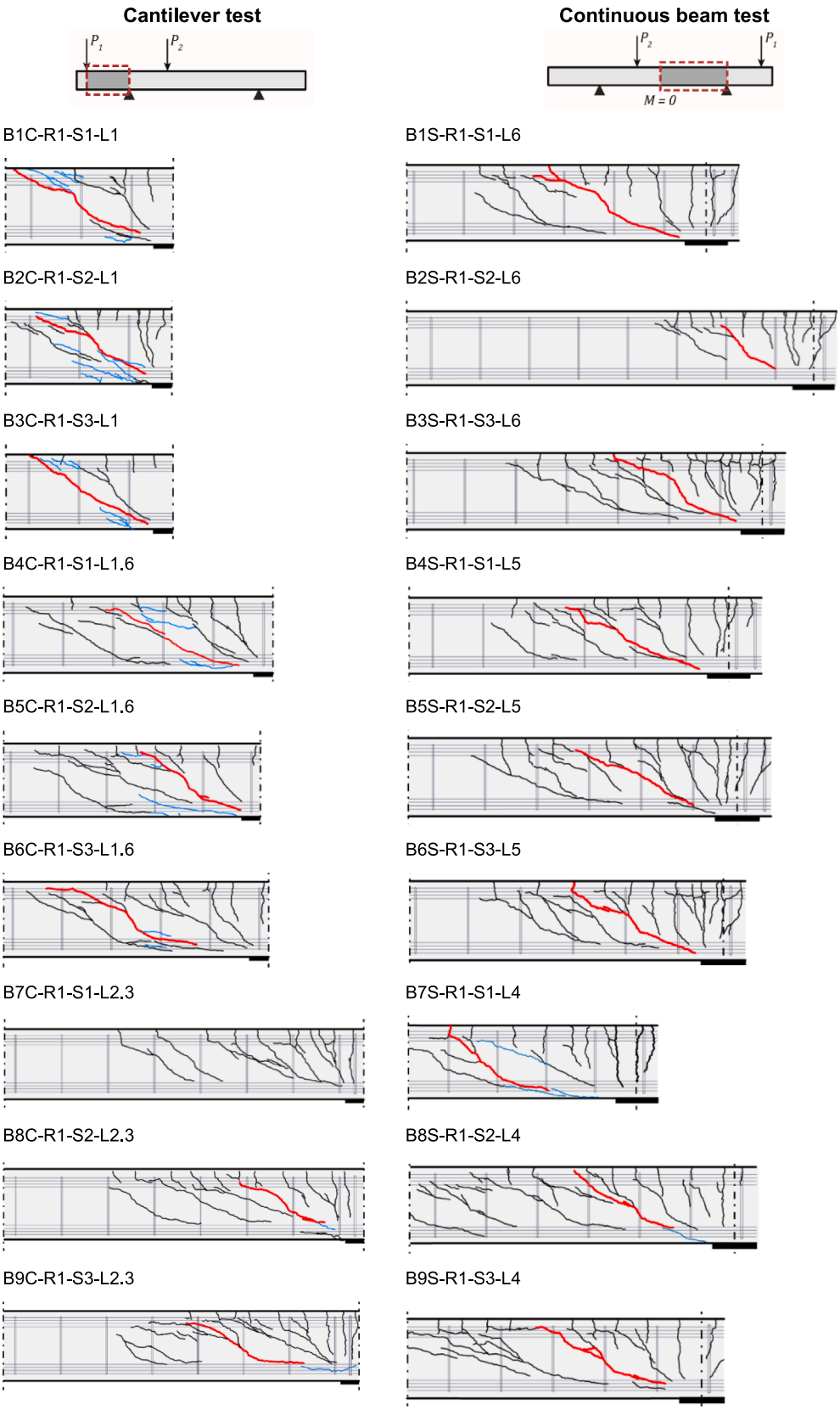

Fig. 7. Observed cracking patterns for the cantilever tests and continuous beam tests of all specimens (test B11S-R0-S2-L4: length represented = 2.00 m [48]; critical shear crack in red and cracks after collapse in blue). (For interpretation of the references to colour in this figure legend, the reader is referred to the web version of this article.)

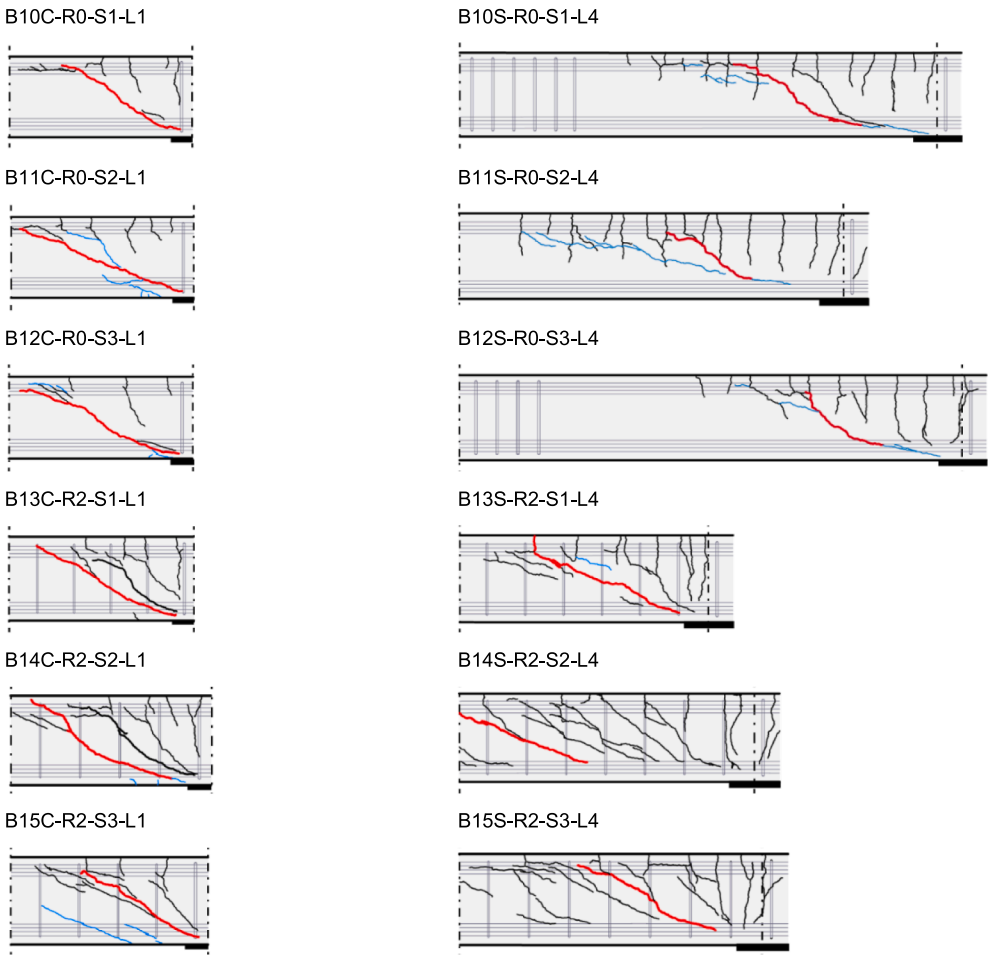

Fig. 7. (*continued*).

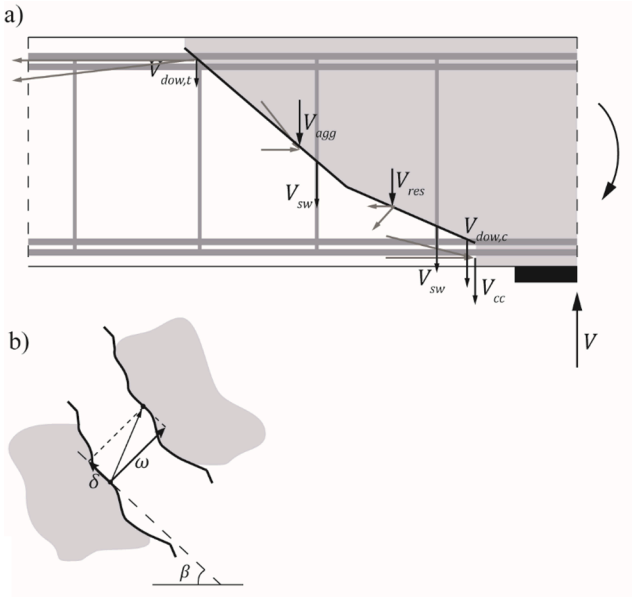

Fig. 8. (a) Analysis of shear-transfer actions: free body defined by the critical shear crack and internal forces (reinforced concrete members with shear reinforcement); (b) critical shear crack kinematics: crack opening and sliding.

For the tested specimens, two stirrups are normally intercepted by the critical shear crack in specimens of series R1, and three in the case of specimens of series R2 (see Fig. 7). Additional stirrups are intercepted by the propagation of the horizontal branch of the critical shear crack at the level of the tensile flexural reinforcement. Nevertheless, those stirrups are not considered in the contribution of the shear reinforcement and their eventual contribution is accounted for in the dowelling forces [44,45]. For the stirrups intercepted in the web, the vertical opening of the critical shear crack ranges from 0.58 mm (test B14C-R2-S2-L1) to 5.24 mm (B6C-R1-S3-L1.6) for the cantilever tests, and from 0.39 mm (test B2S-R1-S2-L6) to 4.39 mm (B1S-R1-S1-L6) for the continuous beam tests. In general, as small crack openings are already sufficient to yield small bar diameters (consistently with Campana et al. [44] and Huber et al. [45]), the stirrups are normally yielded at shear failure, see for instance Fig. 10e for test B1S-R1-S1-L6 (a vertical crack opening of 0.305 mm ensures yielding of the 8-mm diameter stirrup).

3.5. Contribution of compression chord

The concrete compression zone can also transfer shear forces [40]. This action is highly influenced by the shape of the critical shear crack [45,46,55] and is particularly efficient for squat members (but might be very limited for slender ones [16,22]).

Several approaches have been developed so far to assess this capacity [33,34,38]. In this work, the contribution of the compression chord (V_{cc}) is calculated on the basis of the DIC results consistently with the approach developed by Cavagnis et al. [55]. To that aim, the simplified stress field presented in Fig. 11 is considered. The resultant of the forces of the compression zone is composed of a horizontal force (N_{cc}) and a

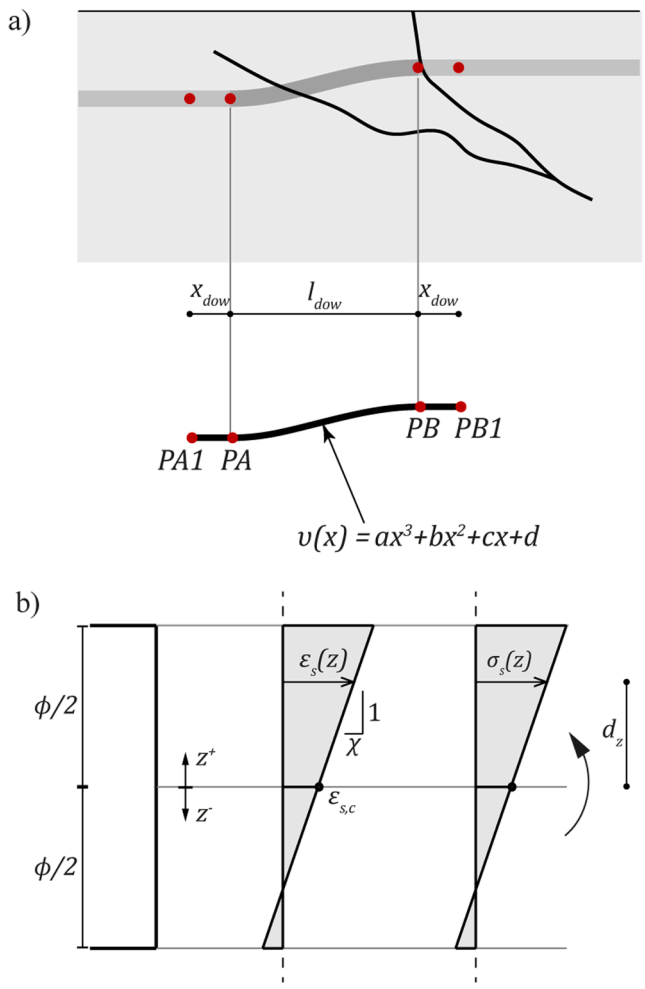

Fig. 9. (a) Dowel action of the flexural reinforcement: deflection of the flexural reinforcement in the horizontal length influenced by this phenomenon [46]; (b) strain and stress distributions of a bar of flexural reinforcement.

vertical one (V_{cc}), which define the inclination of the compression chord (α_{cc}). Accounting for this inclination, forces are transferred between the vertical sections AB (section at the tip of the critical shear crack) and CD (section at the edge of the loading plate). It can be assumed [55] that at the section AB the stress distribution increases linearly from zero at the tip of the crack to the extreme compression fibre, which implies that the resultant of the forces acts at a distance $c_n = 1/3h_T$ from the extreme compression fibre (h_T is the thickness of the compression zone below the tip of the critical shear crack). It can also be assumed [55] that at section CD the stress distribution is almost constant, corresponding to a stress block of thickness c_{m2} with a compressive stress equal to σ_c. According to all these considerations (refer to Fig. 11), the contribution of the compression chord (V_{cc}) results:

$$V_{cc} = N_{cc} \cdot tan\alpha_{cc} = \sigma_c \cdot c_{m2} \cdot b \cdot \frac{1/3 \cdot h_T - c_{m2}/2}{r_T} \quad (10)$$

where b is the width of the section and r_T is the horizontal distance between the vertical sections AB and CD (Fig. 11).

For calculation of V_{cc} (Eq. (10)) the values of the parameters r_T and h_T can be obtained by DIC measurements, but the stress σ_c and the thickness c_{m2} need to be determined. With respect to σ_c, it can be assumed equal to f_c, while c_{m2} can generally be approximated to be equal to c_m (effective depth of the stress block at the edge of the support plate). Both assumptions are consistent with those performed by Cavagnis et al. [55].

4. Analysis of the contribution of the shear-transfer actions to the shear strength

According to the observed crack kinematics and procedures described previously, the contribution of the various shear-transfer actions to the shear strength of the tested specimens is calculated. An interesting property of this approach is that the amount of shear carried by each action can be obtained at any given load step. In particular, at maximum load, this allows determining the most relevant shear transfer actions. This analysis is not performed for test B7C-R1-S1-L2.3 because it fails in bending. The analysis is also not performed in some tests without stirrups (cantilever tests B10C-R0-S1-L1, B11C-R0-S2-L1 and B12C-R0-S3-L1, and continuous beam test B11S-R0-S2-L4) as a consequence of an inaccurate reading of crack kinematics (higher observed errors than expected after DIC analysis). In the case of test B15C-R2-S3-L1, only the contribution of the shear reinforcement is calculated since the inaccurate reading of crack kinematics.

4.1. Analysis of tested specimens

The main results of the contribution of the various shear-transfer actions to the shear strength are presented in Table 4 and Table 5 for the cantilever tests and continuous beam tests respectively. The tables summarize the amount of estimated shear carried by each action at shear failure, including the percentage that they represent of the experimental shear strength $V_{R,test}$ (values in brackets), the sum of the estimated contributions of the different mechanisms ($V_{R,calc}$) and the comparison between the experimental shear strength and the calculated shear strength ($V_{R,test}/V_{R,calc}$). The results are also plotted in Fig. 12 and Fig. 13.

The results show sound agreement between the shear strength obtained from the sum of the estimated contributions and the experimental shear strength for the tested specimens. For members with shear reinforcement, the average of the measured-to-calculated strength results 1.00 for the cantilevers and 1.06 for the continuous beams (with Coefficients of Variation equal to 8.0% and 14.6%, respectively). For continuous beam tests, the average of the measured-to-calculated strength results 1.09 for all tests, both for specimens with and without shear reinforcement (with Coefficient of Variation equal to 15,4%).

By analysing the contribution of the various shear-transfer actions, the following facts can be observed:

- The location, shape and kinematics of the critical shear crack govern the amount of shear carried by aggregate interlock. The contribution of this action varies largely among the tested specimens, but in all of them it is significant in the steeper part of the critical shear crack. This result is in agreement to similar findings obtained by other experimental programmes [46].
- The contribution of the residual tensile strength is not significant for the tested specimens since crack openings are relatively large. It only contributes to the shear strength in four continuous beam tests corresponding to the less slender specimens (L4), two of the series R0 (specimens B10 and B12) and two of the series R1 (specimens B7 and B8). This contribution ranges from 2.1% (B12S-R0-S3-L4) to 8.1% (B10S-R0-S1-L4) of $V_{R,test}$.
- The contribution of the dowel action depends largely on the shape of the critical shear crack, as this action is activated only if the crack intercepts the flexural reinforcement. Overall, in the case of the cantilever tests, the dowel action of both the flexural reinforcement in tension and in compression is significant. Nevertheless, in the continuous beam tests without shear reinforcement, the contribution of the dowel action is more limited (almost negligible) because the shear failure is reached after yielding of the top flexural reinforcement, which severely limits its capacity as dowel. This result in consistent to punching shear cases without transverse reinforcement,

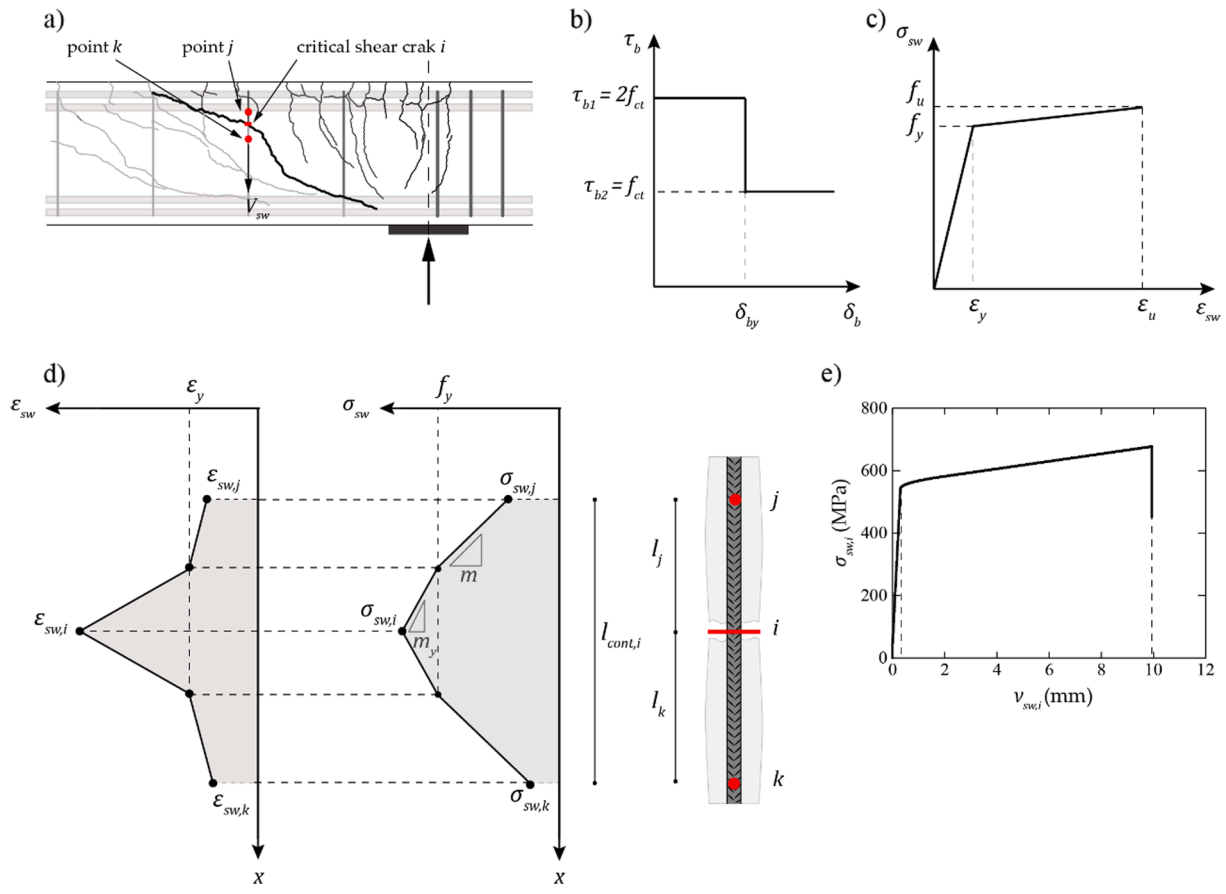

Fig. 10. Shear reinforcement contribution: (a) obtaining the vertical crack opening of the critical shear crack by DIC; (b) the considered rigid-plastic bond behavior; (c) the considered bilinear hardening stress–strain relationship of steel; (d) transmission of stresses and strains in a stirrup (Campana et al. [44]); (e) test B1S-R1-S1-L6, stresses at the location where the critical shear crack intercepts a stirrup according to the vertical crack opening.

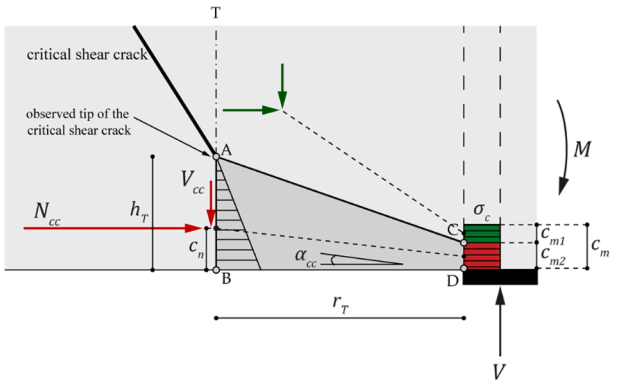

Fig. 11. Hypothesis of the stress field used to determine the contribution of the compression chord (adapted from Cavagnis et al. [55]).

where flexural yielding close to the column region limits or disables the development of dowel action [61]. For the specimens with shear reinforcement, the presence of the stirrups allows however for a higher contribution even after reinforcement yielding.

- Considering the compression chord defined by the location of the observed tip of the critical shear crack, its contribution is strongly influenced by the thickness of the compression zone and shape of the critical shear crack. In the case of the cantilever tests, there is almost no contribution of this action because the critical shear crack intercepts the flexural reinforcement, considerably limiting the thickness of the compression zone in all the test (see Fig. 7). However, there are some exceptions in which the limited development of the critical shear crack allows for the inclination of the compression chord (see Fig. 7). This is the case of the continuous beam tests in specimens of series R0 (specimens B10 and B12), with a contribution of this mechanism about 5.0% of $V_{R,test}$, and the test B2S-R1-S2-L6 of the series R1, with a significant contribution equal to 16.1% of $V_{R,test}$.
- In the case of specimens with shear reinforcement, the critical shear crack also plays an instrumental role for the contribution of the stirrups to the shear strength, as its shape determines the number of stirrups activated and its kinematics the amount of shear carried by them (see Fig. 7). For the tested specimens with shear reinforcement, the contribution of this mechanism is governing. The contribution of the shear reinforcement is higher in the specimens of series R2 (ϕ8/20) than in those of series R1 (ϕ8/30), because three stirrups are intercepted by the critical shear crack for series R2 while two are intercepted for series R1. However, the relative significance of this contribution with respect to the experimental shear strength is comparable regardless of the amount of shear reinforcement. It ranges from 48.1% (B8S-R1-S2-L4) to 88.8% (B4S-R1-S1-L5) of $V_{R,test}$ for the specimens of the series R1, and from 61.9% (B15C-R2-S3-L1) to 87.6% (B15S-R2-S3-L4) of $V_{R,test}$ for the specimens of the series R2.

It is interesting to note that for members with stirrups, even if the stirrup contribution is governing, a fraction of the total shear is still carried by the remaining shear-transfer actions (notably the aggregate interlock and dowel action). This implies that the angle of the compression field developing in the web is flatter than the corresponding angle of the cracks (and is thus intercepted by them). This observation is in agreement with the considerations performed by limit

Table 4
Contribution of the various shear-transfer actions to the shear strength for the cantilever tests.

Cantilever test	V_{agg}(kN)	V_{res}(kN)	$V_{dow,t}$(kN)	$V_{dow,c}$(kN)	V_{cc}(kN)	V_s(kN)	$V_{R,calc}$(kN)	$V_{R,test}$(kN)	$V_{R,test}/V_{R,calc}$
B1C-R1-S1-L1	2.5 (1.3)	0.0	16.9 (8.6)	53.8 (27.4)	0.0	123.7 (62.9)	196.9	196.8	1.00
B2C-R1-S2-L1	8.2 (3.8)	0.0	26.6 (12.4)	51.0 (23.8)	0.0	118.1 (55.0)	204.0	214.6	1.05
B3C-R1-S3-L1	13.0 (6.3)	0.0	43.5 (21.1)	55.4 (26.9)	0.0	116.7 (56.6)	228.7	206.3	0.90
B4C-R1-S1-L1.6	4.0 (2.3)	0.0	36.8 (21.1)	37.5 (21.5)	0.0	118.3 (67.9)	196.6	174.2	0.89
B5C-R1-S2-L1.6	16.0 (7.4)	0.0	31.4 (14.6)	28.2 (13.1)	0.0	119.1 (55.4)	194.7	215.2	1.11
B6C-R1-S3-L1.6	2.5 (1.2)	0.0	32.9 (15.8)	30.3 (14.6)	0.0	120.1 (57.8)	185.8	207.6	1.12
B8C-R1-S2-L2.3	35.9 (21.4)	0.0	32.3 (19.3)	0.4 (0.3)	0.0	111.4 (66.4)	180.0	167.6	0.93
B9C-R1-S3-L2.3	12.2 (8.2)	0.0	15.5 (10.4)	3.7 (2.5)	0.0	112.4 (75.6)	143.8	148.7	1.03
B13C-R2-S1-L1	6.4 (2.7)	0.0	25.3 (10.8)	28.5 (12.1)	0.0	176.2 (75.0)	236.4	235.0	0.99
B14C-R2-S2-L1	14.7 (2.5)	0.0	61.6 (23.0)	21.1 (7.9)	0.0	171.9 (64.2)	269.9	267.7	0.99
B15C-R2-S3-L1	NA	NA	NA	NA	NA	174.0 (61.9)	NA	281.0	NA
								Mean	*1.00*
								CoV	*8.0%*

Note: values at shear failure; the values in brackets refer to the percentage of the shear-transfer action with respect to the experimental shear strength $V_{R,test}$; NA (not available data).

Table 5
Contribution of the various shear-transfer actions to the shear strength for the continuous beam tests.

Continuous beam test	V_{agg}(kN)	V_{res}(kN)	$V_{dow,t}$(kN)	$V_{dow,c}$(kN)	V_{cc}(kN)	V_s(kN)	$V_{R,calc}$(kN)	$V_{R,test}$(kN)	$V_{R,test}/V_{R,calc}$
B1S-R1-S1-L6	0.9 (0.7)	0.0	0.2 (0.1)	29.0 (20.8)	0.0	121.2 (86.9)	151.3	139.4	0.92
B2S-R1-S2-L6	21.8 (15.3)	0.0	0.1 (0.0)	0.0	22.9 (16.1)	111.7 (78.4)	156.4	142.4	0.91
B3S-R1-S3-L6	5.5 (3.8)	0.0	21.6 (14.9)	25.0 (17.2)	0.0	124.0 (85.4)	176.1	145.1	0.82
B4S-R1-S1-L5	0.4 (0.3)	0.0	3.8 (2.7)	29.7 (20.8)	0.0	127.0 (88.8)	160.9	143.1	0.89
B5S-R1-S2-L5	2.6 (1.4)	0.0	16.5 (8.7)	32.4 (17.2)	0.0	119.7 (63.4)	171.2	188.7	1.10
B6S-R1-S3-L5	13.7 (7.2)	0.0	0.3 (0.1)	21.7 (11.3)	0.0	116.4 (61.0)	151.9	190.8	1.26
B7S-R1-S1-L4	43.0 (19.9)	10.6 (4.9)	2.3 (1.1)	8.7 (4.0)	0.0	116.8 (54.0)	181.4	216.3	1.19
B8S-R1-S2-L4	35.7 (17.8)	8.0 (4.0)	9.4 (4.7)	11.8 (5.9)	0.0	96.7 (48.1)	161.6	200.9	1.24
B9S-R1-S3-L4	14.0 (7.3)	0.0	8.6 (4.4)	14.8 (7.7)	0.0	116.8 (60.7)	154.1	192.3	1.25
B10S-R0-S1-L4	45.6 (55.4)	6.7 (8.1)	2.5 (3.0)	0.4 (0.4)	4.4 (5.3)	0.0	59.5	82.4	1.38
B12S-R0-S3-L4	63.5 (72.5)	1.8 (2.1)	0.1 (0.1)	2.2 (2.5)	4.5 (5.2)	0.0	72.1	87.6	1.21
B13S-R2-S1-L4	13.0 (6.0)	0.0	8.3 (3.8)	24.8 (11.4)	0.0	175.3 (80.6)	221.4	217.6	0.98
B14S-R2-S2-L4	8.5 (3.8)	0.0	17.4 (7.8)	0.0	0.0	172.0 (77.3)	197.9	222.5	1.12
B15S-R2-S3-L4	4.7 (2.4)	0.0	1.2 (0.6)	3.9 (1.9)	0.0	174.5 (87.6)	184.3	199.1	1.08
								Mean	*1.09*
								CoV	*15.4%*

Note: values at shear failure; the values in brackets refer to the percentage of the shear-transfer action with respect to the experimental shear strength $V_{R,test}$.

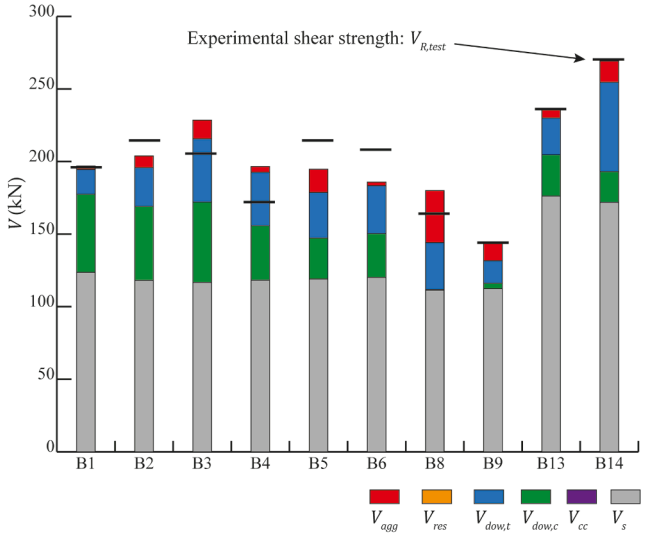

Fig. 12. Contribution of the various shear-transfer actions to the shear strength for the cantilever tests (specimens not included: B7 (bending failure); B10-B12 and B15 (inaccurate reading of crack kinematics)).

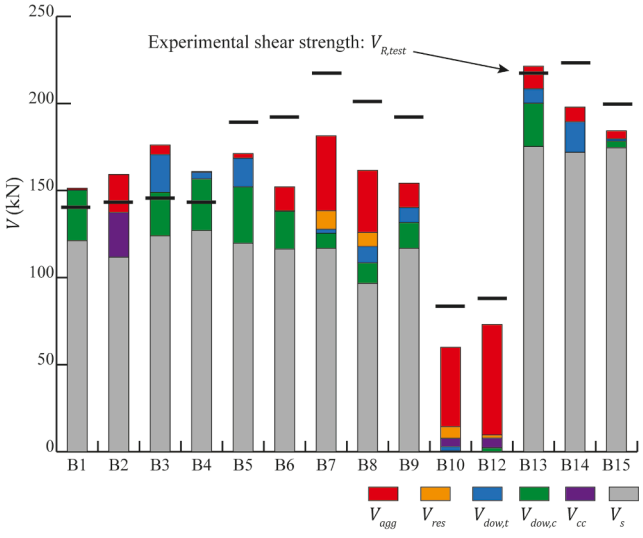

Fig. 13. Contribution of the various shear-transfer actions to the shear strength for the continuous beam tests (specimen not included: B11 (inaccurate reading of crack kinematics)).

analysis [62] or the MCFT [7].

4.2. Considerations for the cantilever tests

In addition to the previous considerations, the following conclusions about the governing shear-transfer actions at shear failure are drawn for the cantilever tests:

- Specimens with shear reinforcement (shear failure before yielding of the flexural reinforcement).

The contribution of the shear reinforcement is governing (up to 75.0% of $V_{R,test}$ in B13C-R2-S1-L1, Fig. 14). This is influenced to a large extent by the shape of the critical shear crack, which develops in a relatively flat manner, intercepting a large number of stirrups. It is also quite relevant the contribution of the dowelling action, both in tension (23.0% of $V_{R,test}$ in B14C-R2-S2-L1) and compression (27.4% of $V_{R,test}$ in B1C-R1-S1-L1), because the critical shear crack intercepts both the tensile and the compressive flexural reinforcement. With respect to aggregate interlock, this contribution is limited accounting to the relatively large crack widths (refer to the decreasing significance of this action in Fig. 14).

- Specimens with shear reinforcement (shear failure after yielding of the flexural reinforcement).

The contribution of the shear reinforcement is also governing (66.4% and 75.6% of $V_{R,test}$ in B8C-R1-S2-L2.3 and B9C-R1-S3-L2.3, respectively). The aggregate interlock and the dowelling action of the tensile reinforcement are also not negligible and contribute for a similar percentage to the shear strength (up to 21.4% and 19.3% of $V_{R,test}$ in B8C-R1-S2-L2.3, respectively, Fig. 15). This fact is justified by the shape of the critical shear crack. This crack is generally steeper than when failure develops prior to the yielding of the flexural reinforcement (see Fig. 14 and Fig. 15). This is due to the fact that yielding of the reinforcement localizes the strains in the vicinity of the support (plastic hinge region), leading to larger crack widths in this region and thus to more unfavourable resistances. Such steeper shape is however more prone to aggregate interlock engagement and activates a lower number of stirrups (compare Fig. 14 and Fig. 15).

4.3. Consideration for continuous beam tests

For the continuous beam tests, the following conclusions about the governing shear-transfer actions at shear failure are drawn:

- Specimens without shear reinforcement (shear failure after the development of one plastic hinge).

The contribution of the aggregate interlock is governing (up to 72.5% of $V_{R,test}$ in B12S-R0-S3-L4, Fig. 16). This is due to the limited opening of the critical shear crack, combined with the crack sliding due to the shape of the crack. According to the low crack openings, residual tensile stresses also contribute to the transfer of shear forces near the tip of the crack. Its overall contribution is however lower than for aggregate interlock (less than 10% of $V_{R,test}$). As a result of the limited extension of the critical shear crack (it does not intercept the bottom flexural reinforcement), the contribution of the dowelling action in compression is negligible, but the compression chord can contribute to the shear strength (about 5.0% of $V_{R,test}$ in both B10S-R0-S1-L4 and B12S-R0-S3-L4).

- Specimens with shear reinforcement (shear failure after development of one plastic hinge).

The contribution of the shear reinforcement is governing (up to 88.8% of $V_{R,test}$ in B4S-R1-S1-L5). For the specimens of series R1, the contribution of the aggregate interlock is also notable (up to 19.9% of $V_{R,test}$ in B7S-R1-S1-L4, Fig. 17). This is explained by the presence of rather steep segments in the critical shear crack allowing for an enhanced engagement of interlock stresses (see Fig. 17). Also, dowel action of the flexural reinforcement in compression is notable (up to 20.8% of $V_{R,test}$ in B4S-R1-S1-L5). The residual tensile strength shows a limited contribution in specimens B7 and B8 (less than 5% of $V_{R,test}$). For the specimens of series R2, the aggregate interlock and the dowel action in compression are more limited than in the series R1 (less than 12% of $V_{R,test}$ both of them).

- Specimens with shear reinforcement (shear failure after development of two plastic hinges).

The contribution of the shear reinforcement is again governing (up to 86.9% of $V_{R,test}$ in B1S-R1-S1-L6). In general, the contribution of aggregate interlock is negligible due to the large crack openings, but the contribution of the dowel action in compression is relatively high (up to 20.8% of $V_{R,test}$ in B1S-R1-S1-L6) since the crack intercepts the bottom flexural reinforcement. In the case of the test B2S-R1-S2-L6 (Fig. 18), the shape of the critical shear crack is rather steep (intercepting a limited number of stirrups) and its opening is more limited. As a result, the aggregate interlock plays a more significant role (15.3% of $V_{R,test}$) and the thickness of the compression zone allows the compression chord to contribute for a significant percentage to the shear strength (16.1% of $V_{R,test}$).

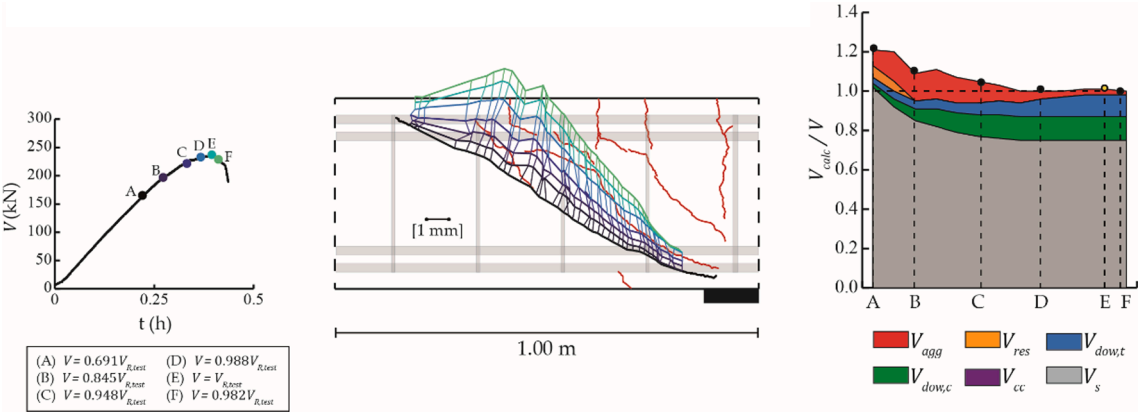

Fig. 14. Test B13C-R2-S2-L1: development of the cracking at selected load steps (shear failure occurs at the step (E)) and the corresponding contributions of the various shear-transfer actions.

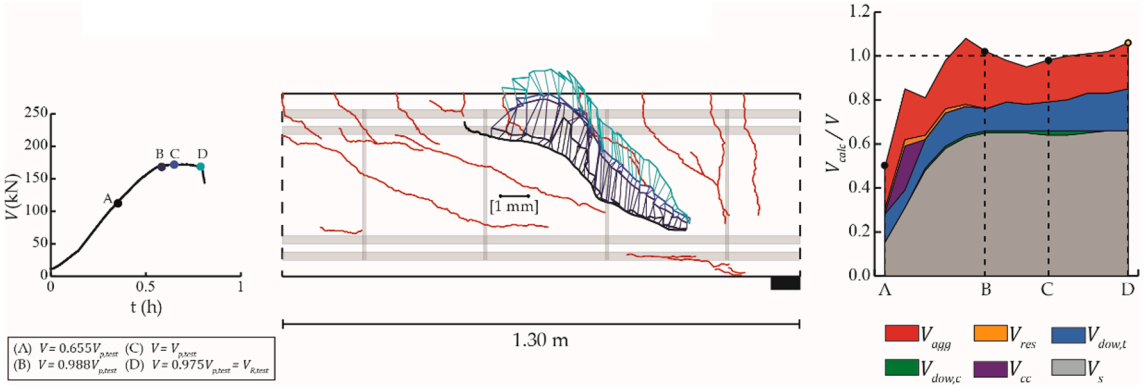

Fig. 15. Test B8C-R1-S2-L2.3: development of the cracking at selected load steps (shear failure occurs at the step (D)) and the corresponding contributions of the various shear-transfer actions ($V_{p.test}$ is the shear at the peak load of the test).

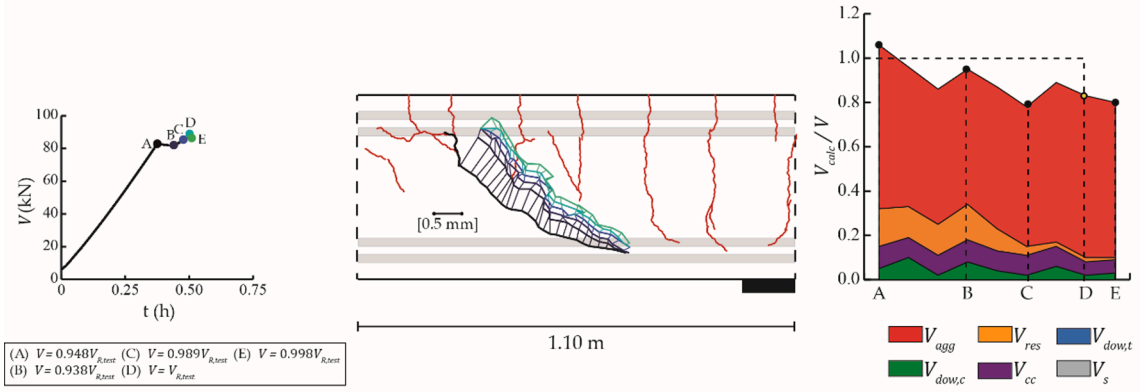

Fig. 16. Test B12S-R0-S3-L4: development of the cracking at selected load steps (shear failure occurs at the step (D)) and the corresponding contributions of the various shear-transfer actions (step load (A) corresponds to the development of the plastic hinge).

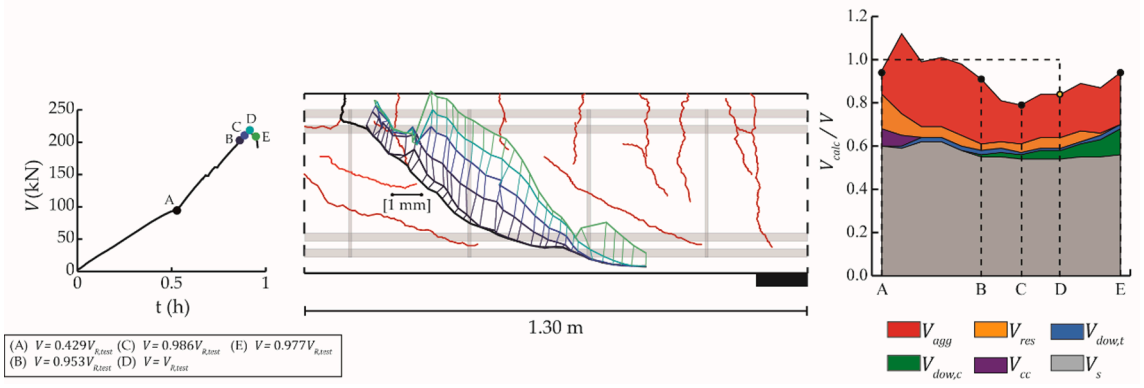

Fig. 17. Test B7S-R1-S1-L4: development of the cracking at selected load steps (shear failure occurs at the step (D)) and the corresponding contributions of the various shear-transfer actions (step load (A) corresponds to the development of the plastic hinge).

5. Conclusions

In this paper, a detailed investigation of the contribution of the various potential shear-transfer actions to the shear strength of reinforced concrete beams with and without shear reinforcement is presented. On the basis of the detailed crack kinematics, obtained from the DIC measurements, the shear strength of the tests is estimated using suitable constitutive models and calculation methodologies. The specimens of the experimental programme were designed to represent realistic conditions of reinforced concrete structures, with special emphasis on developing shear failures after yielding of the flexural reinforcement.

The main conclusions from this investigation are the following:

1. At failure, the sum of the contribution of each shear-transfer action adequately explains the experimental values of shear strength obtained for each specimen, validating the analysis procedure.
2. The contribution of each shear-transfer action to the shear strength is strongly influenced by cracking patterns and particularly by the location, shape and kinematics of the critical shear crack. The presence or absence of stirrups is highly influencing this pattern. Shear reinforcement leads to more uniformly distributed inclined cracks,

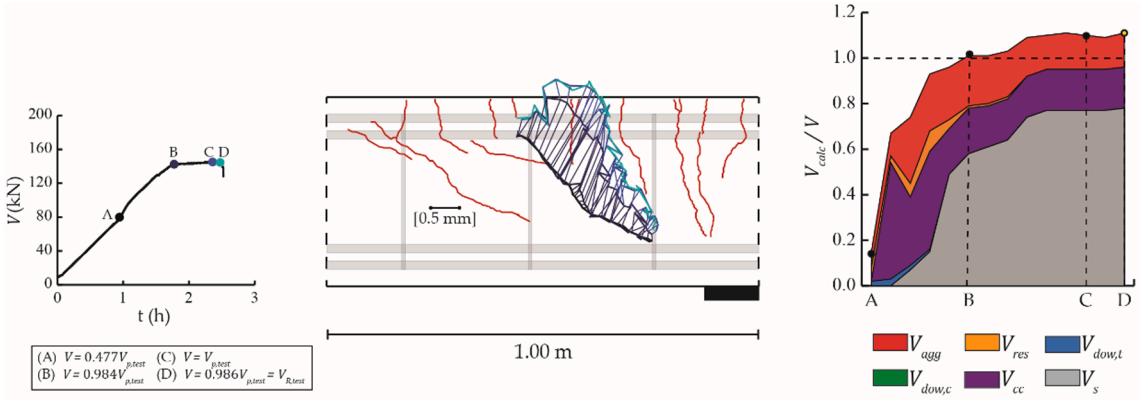

Fig. 18. Test B2S-R1-S2-L6: development of the cracking at selected load steps (shear failure occurs at the step (D)) and the corresponding contributions of the various shear-transfer actions ($V_{p,test}$ is the shear at the peak load of the test; step loads (A) and (B) correspond to the development of the first and the second plastic hinges, respectively).

whereas strains localize in a single critical shear crack in specimens without stirrups.

3. Development of yielding in the flexural reinforcement influences significantly the shear-transfer actions. When flexural reinforcement yields, the critical shear crack is steeper (due to the localization of strains at the plastic hinge region), which allows for the activation of a lower number of stirrups and a higher engagement of aggregate interlock.
4. The results consistently show that dowel action reduces significantly for yielded reinforcement and low openings of the critical shear crack. It can however be significant for members with stirrups. In general, an increase of critical shear crack openings implies a reduction of the force transferred by aggregate interlocking, but an increase of the shear transferred by the dowel action.
5. The shear force carried by the inclined compression chord depends significantly on the location of the tip of the critical shear crack. Considering the compression chord defined by the location of the observed tip of the critical shear crack, its contribution is negligible in all tests except in the continuous beam tests without shear reinforcement.
6. In the specimens with stirrups, the shear reinforcement contribution is dominant. The crack pattern determines the number of stirrups accounted for contributing to shear strength and the shear force transferred by each of them. The relative contribution of this action to shear strength is comparable regardless of the shear reinforcement ratio of specimens. Also, despite the fact that this contribution is governing for the strength, a fraction of the total shear force is still carried by aggregate interlock and dowel action. This indicates, particularly for the engagement of aggregate interlock, a flatter angle of the compression field than that of the critical shear crack.

Declaration of Competing Interest

The authors declare that they have no known competing financial interests or personal relationships that could have appeared to influence the work reported in this paper.

Acknowledgements

This research was funded by grants from the Spanish Ministry of Economy and Competitiveness to Research Project BIA2015-64672-C4-4-R. The experimental programme was developed in the Laboratory of Concrete at the Institute of Concrete Science and Technology (ICITECH) of the Universitat Politècnica de València (UPV), with concrete supplied by Caplansa. Andrea Monserrat was supported by the Conselleria d'Educació, Investigació, Cultura i Esport of the Generalitat Valenciana (Order 6/2015, DOGV no. 7615 15.09.2015) with European Regional Development Funds (ERDF) allocated by the EU. VIC2D software was employed during the research stay of Andrea Monserrat at the EPFL (Lausanne, Switzerland).

References

[1] Schlaich J, Shafer K, Jennewein M. Toward a consistent design of structural concrete. PCI Journal 1987;32:74–150.
[2] Schlaich J, Schäfer K. Design and detailing of structural concrete using strut-and-tie models. Struct Eng 1991;69(6):113–25.
[3] Ritter W. Die Bauweise Hennebique (The Hennebique system). Schweizerische Bauzeitung; 1899.
[4] Mörsch E. Der Eisenbetonbau, seine Theorie und Anwendung (Reinforced concrete, theory and application). Stuttgart: Wayss & Freytag; 1902.
[5] Mörsch E. Der Eisenbetonbau (Concrete-steel construction). New York: McGraw-Hill; 1909.
[6] Muttoni A, Schwartz J, Thürlimann B. Design of Concrete Structures with Stress Fields. Birkhaüser / Springer; 1997.
[7] Vecchio FJ, Collins MP. The Modified Compression-Field Theory for reinforced concrete elements subjected to shear. J Proc 1986;83(2):219–31.
[8] Bentz E, Vecchio FJ, Collins MP. Simplified Modified Compression Field Theory of calculating shear strength of reinforced concrete elements. ACI Struct J 2006;103 (4):614–24.
[9] Pang X-BD, Hsu TTC. Behavior of reinforced concrete membrane elements in shear. ACI Struct J 1995;92(6):665–79.
[10] Pang X-BD, Hsu TTC. Fixed-Angle Softened-Truss Model for reinforced concrete. ACI Struct J 1996;93(2):197–207.
[11] Dei Poli S, Gambarova PG, Karakoç C. Aggregate interlock role in RC thin-webbed beams in shear. J Struct Eng 1987;113(1):1–19.
[12] Reineck K-H. Modelling of members with transverse reinforcement. IABSE Colloq Struct Concr 1991;62:481–8.
[13] EN 1992-1-1:2004. Eurocode 2: Design of concrete structures – Part 1-1: General rules and rules for buildings.
[14] ACI Committee 318. Building code requirements for structural concrete (ACI 318-19); and commentary (ACI 318R-19). American Concrete Institute; 2019.
[15] Fenwick RC, Paulay T. Mechanism of shear resistance of concrete beams. J Struct Div 1968;94(10):2325–50.
[16] Taylor H. Investigation of the forces carried across cracks in reinforced concrete beams in shear by inlerlock of aggregate. London (UK) 1970.
[17] Paulay T, Loeber PJ. Shear transfer by aggregate interlock. ACI Spec Publ SP-42, Shear Reinf Concr 1974;1:1–16.
[18] Bažant ZP, Gambarova PG. Rough cracks in reinforced concrete. J Struct Div 1980; 106(4):819–42.
[19] Walraven JC. Fundamental analysis of aggregate interlock. ASCE J Struct Div 1981; 107(11):2245–70.
[20] Ulaga T. Betonbauteile mit Stab- und Lamellenbewehrung: Verbund- und Zuggliedmodellierung. ETH Zürich; 2003.
[21] Guidotti R. Poinçonnement des planchers-dalles avec colonnes superposées fortement sollicitées. Lausanne, Switzerland: École Polytechnique Fédérale de Lausanne; 2010.
[22] Sagaseta J, Vollum RL. Influence of aggregate fracture on shear transfer through cracks in reinforced concrete. Mag Concr Res 2011;63(2):119–37.
[23] Krefeld W, Thurston CW. Contribution of longitudinal steel to shear resistance of reinforced concrete beams. ACI J Proc 1966;63(3):325–44.
[24] Taylor H. Investigation of the dowel shear forces carried by the tensile steel in reinforced concrete beams. London (UK) 1969.
[25] Baumann T, Rüsch H. Versuche zum Studium der Ver-dübelungswirkung der Biegezugbewehrung eines Stahlbetonbalkens. Berlin: Ernst; 1970.

[26] Chana PS. Investigation of the mechanism of shear failure of reinforced concrete beams. Mag Concr Res 1987;39(141):196–204.
[27] Dei Poli S, Di Prisco M, Gambarova PG. Cover and stirrup effects on the shear response of dowel bar embedded in concrete. Struct J 1993;90(4):441–50.
[28] Zararis PD. Shear strength and minimum shear reinforcement of reinforced concrete slender beams. Struct J 2003;100(2):203–14.
[29] Hillerborg A, Modéer M, Petersson P-E. Analysis of crack formation and crack growth in concrete by means of fracture mechanics and finite elements. Cem Concr Res 1976;6(6):773–81.
[30] Reinhardt HW. Plain concrete modeled as an elastic strain-softening material at fracture. Eng Fract Mech 1985;22(5):787–96.
[31] Hordijk DA. Tensile and tensile fatigue behaviour of concrete; experiments, modelling and analyses. Heron 1992;37(1):1–79.
[32] Tureyen AK, Frosch RJ. Concrete shear strength: another perspective. Struct J 2003;100(5):609–15.
[33] Park H-G, Choi K-K, Wight JK. Strain-based shear strength model for slender beams without web reinforcement. ACI Struct J 2006;103(6):783–93.
[34] Zararis PD, Papadakis GC. Diagonal shear failure and size effect in RC beams without web reinforcement. J Struct Eng 2001;127(7):733–42.
[35] Wolf TS, Frosch RJ. Shear design of prestressed concrete: A unified approach. J Struct Eng 2007;133(11):1512–9.
[36] Choi KK, Park HG, Wight JK. Unified shear strength model for reinforced concrete beams – Part I: Development. ACI Struct J 2007;104(2):142–52.
[37] Bažant ZP, Yu Q, Gerstle W, Hanson J, Ju JW. Justificacion of ACI 446 Proposal for Updating ACI Code Provisions for shear design of reinforced concrete beams. Struct J 2007;104(5):601–10.
[38] Marí A, Bairán J, Cladera A, Oller E, Ribas C. Shear-flexural strength mechanical model for the design and assessment of reinforced concrete beams. Struct Infrastruct Eng 2015;11(11):1399–419.
[39] Yu Q, Le J-L, Hubler MH, Wendner R, Cusatis G, Bažant ZP. Comparison of main models for size effect on shear strength of reinforced and prestressed concrete beams. Struct Concr 2016;17(5):778–89.
[40] Cladera A, Marí A, Bairán JM, Ribas C, Oller E, Duarte N. The compression chord capacity model for the shear design and assessment of reinforced and prestressed concrete beams. Struct Concr 2017;17(6):1017–32.
[41] Muttoni A, Fernández Ruiz M. Shear strength of members without transverse reinforcement as function of critical shear crack width. ACI Struct J 2008;105(2):163–72.
[42] Cavagnis F, Simões J, Fernández Ruiz M, Muttoni A. Shear strength of members without transverse reinforcement based on development of critical shear crack. ACI Struct J, Jan 2020;117:103–18.
[43] Marí A, Bairán J, Cladera A, Oller E. Shear design and assessment of reinforced and prestressed concrete beams based on a mechanical model. J Struct Eng 2016;142(10).
[44] Campana S, Fernández Ruiz M, Anastasi A, Muttoni A. Analysis of shear-transfer actions on one-way RC members based on measured cracking pattern and failure kinematics. Mag Concr Res 2013:386–404.
[45] Huber P, Huber T, Kollegger J. Investigation of the shear behavior of RC beams on the basis of measured crack kinematics. Eng Struct 2016;113:41–58.
[46] Cavagnis F, Fernández Ruiz M, Muttoni A. An analysis of the shear-transfer actions in reinforced concrete members without transverse reinforcement based on refined experimental measurements. Struct Concr 2018;19(1):49–64.
[47] Monserrat López A, Miguel Sosa P, Bonet Senach JL, Fernández Prada MA. Influence of the plastic hinge rotations on shear strength in continuous reinforced concrete beams with shear reinforcement. Eng Struct 2020;207:110242.
[48] Monserrat López A, Miguel Sosa P, Bonet Senach JL, Fernández Prada MA. Experimental study of shear strength in continuous reinforced concrete beams with and without shear reinforcement. Eng Struct 2020;220:110967.
[49] Islam MS, Pam HJ, Kwan AKH. Shear capacity of high-strength concrete beams with their point of inflection within the shear span. Proc Inst Civ Eng Struct Build 1998;128(1):91–9.
[50] Collins MP, Kuchma D. How safe are our large, lightly reinforced concrete beams, slabs, and footings? ACI Struct J 1999;96(4):482–90.
[51] Vaz Rodrigues R, Muttoni A, Fernández Ruiz M. Influence of shear on rotation capacity of reinforced concrete members without shear reinforcement. ACI Struct J 2010;107(5):516–25.
[52] Tung ND, Tue NV. Effect of support condition and load arrangement on the shear response of reinforced concrete beams without transverse reinforcement. Eng Struct 2016;111:370–82.
[53] Adam V, Classen M, Hillebrand M, Hegger J. Shear in continuour slab segments without shear reinforcement under distributed loads.. fib Symposium; 2019.
[54] Vic-2D Reference Manual 2009.
[55] Cavagnis F, Fernández Ruiz M, Muttoni A. A mechanical model for failures in shear of members without transverse reinforcement based on development of a critical shear crack. Eng Struct 2018;157:300–15.
[56] Model Code 2010. Fédération International du Béton (fib); 2012.
[57] Fernández Ruiz M, Muttoni A, Sagaseta J. Shear strength of concrete members without transverse reinforcement: A mechanical approach to consistently account for size and strain effects. Eng Struct 2015;99:360–72.
[58] Taylor HPJ. The fundamental behavior of reinforced concrete beams in bending and shear. ACI Spec Publ 1974;42:43–78.
[59] Sigrist V. Zum Verformungsvermögen von Stahlbetonträgern (Deformation capacity of reinforced concrete beams). ETH Zürich; 1995.
[60] Fernández Ruiz M, Muttoni A, Gambarova PG. Analytical modeling of the pre- and postyield behavior of bond in reinforced concrete. J Struct Eng 2007;133(10):1364–72.
[61] Simões JT, Fernández Ruiz M, Muttoni A. Validation of the Critical Shear Crack Theory for punching of slabs without transverse reinforcement by means of a refined mechanical model. Struct Concr 2018;19(1):191–216.
[62] Nielsen MP, Hoang LC. Limit analysis and concrete plasticity. CRC Press; 1999.